An Alternative to Conventional λ-Intermediate States in Alchemical Free Energy Calculations: λ-Enveloping Distribution Sampling.

Gerhard König,* Nina Glaser, Benjamin Schroeder, Alžbeta Kubincová, Philippe H. Hünenberger, and Sereina Riniker*

Laboratory of Physical Chemistry, Department of Chemistry and Applied Biosciences, ETH Zürich, Vladimir-Prelog-Weg 2, 8093 Zürich, Switzerland

E-mail: gerhard.koenig@phys.chem.ethz.ch; sriniker@ethz.ch

Abstract

Alchemical free energy calculations typically rely on intermediate states to bridge between the relevant phase spaces of the two end states. These intermediate states are usually created by mixing the energies or parameters of the end states according to a coupling parameter λ. The choice of the procedure has a strong impact on the efficiency of the calculation, as it affects both the encountered energy barriers and the phase space overlap between the states. The present work builds on the connection between the minimum variance pathway (MVP) and enveloping distribution sampling (EDS). It is shown that both methods can be regarded as special cases of a common scheme referred to as λ-EDS, which can also reproduce the behavior of conventional λ-intermediate states. A particularly attractive feature of λ-EDS is its ability to emulate the use of soft core potentials while avoiding the associated computational overhead when applying efficient free energy estimators such as the multistate Bennett's acceptance ratio (MBAR). The method is illustrated for both relative and absolute free

energy calculations considering five benchmark systems. The first two systems (charge inversion and cavity creation in a dipolar solvent) demonstrate the use of λ-EDS as an alternative coupling scheme in the context of thermodynamic integration (TI). The three other systems (change of bond length, change of dihedral angles, and cavity creation in water) investigate the efficiency and optimal choice of parameters in the context of free energy perturbation (FEP) and Bennett's acceptance ratio (BAR). It is shown that λ-EDS allows larger steps along the alchemical pathway than conventional intermediate states.

Introduction

The calculation of free energy differences based on atomistic molecular dynamics (MD) simulations[1–3] has become an essential tool in computational chemistry, molecular biology, material sciences, and drug design. However, these methods are computationally expensive because of the required conformational sampling[4–6] and the need for sufficient phase space overlap.[7–9] To calculate the free energy difference between an initial state A and a final state B, these end states are commonly connected with a coupling parameter λ, which varies from 0 to 1. The λ-parameter is used to create a hybrid Hamiltonian $H(\lambda)$ that yields the end state Hamiltonians as $H(0) = H_A$ and $H(1) = H_B$. This procedure is referred to as multi-configuration,[10,11] staged,[7,8,12,13] or stratified[14] sampling. Depending on the selected protocol, there can be one[15–18] or many[4,19–21] intermediate states, and their simulation often dominates for the computational costs.

The simplest choice for generating λ-states is energy interpolation (EI), which goes back to the thermodynamic integration (TI) approach by Kirkwood in 1935.[22,23] It defines $H(\lambda)$ as a linear combination of the physical end state Hamiltonians. Another variant, referred to as parameter interpolation (PI),[10,24,25] performs the combination in terms of the individual force field parameters. The application of PI requires only one potential energy evaluation per timestep, which decreases the computational costs of the simulation. The scheme does

not require dedicated free energy code, as the λ-combined parameters can be created externally and fed to a standard simulation program.[26,27] However, this comes at the cost of more postprocessing effort, as energies at other λ-points have to be calculated explicitly for estimators such as free energy perturbation (FEP, also known as the Zwanzig equation or the exponential formula),[23,28] Bennett's acceptance ratio (BAR),[29,30] or the multistate BAR (MBAR) method.[31] Free energy differences in conformational space are usually calculated with umbrella sampling,[32] which involves artificial intermediate states where conformations are restrained by adding biasing potentials.

A shortcoming of both the EI and PI approaches are divergent free energy results and unstable simulations if atoms are converted to noninteracting dummy atoms. This is known as the van der Waals endpoint problem.[25,26,33–36] Its primary cause are steric clashes during the decoupling of dummy atoms. Different approaches have been developed to address this issue. In the sprouting scheme,[37–39] new atoms are grown inside existing ones before extending the corresponding bond. The serial insertion approach[26,40,41] involves growing the atoms successively in full steps, and using BAR as an estimator. The scheduling method[42,43] relies on optimizing the sequence and functional form for the scaling of individual force field terms within an EI framework. The most common approach to deal with the van der Waals endpoint problem are soft core potentials (SCP).[35,36,44–50] These rely on λ-dependent potential energies that still satisfy the limiting conditions $H_A(0) = H_A$ and $H_B(1) = H_B$ at the end points, but soften the repulsion at intermediate λ-points. Singularities are avoided because their pairwise interactions remain finite at zero distance. However, SCP require dedicated code in the simulation program and lead to computational overhead when applying estimators such as FEP, BAR, or MBAR, as additional potential energy evaluations are required for the postprocessing of all λ-points.

Valleau and Card recognized in 1972 that the main purpose of intermediate states is to provide a "bridging distribution" that has sufficient overlap with the phase spaces of the two end states.[12] This distribution can be tailored to maximize efficiency, and does not have

to follow the shapes of the probability distributions of the end states. This idea inspired Bennett's eminent paper from 1976,[29] in which he also suggested to use "an appropriately weighted log mean exponential of a sequence of overlapping potentials" to generate intermediate ensembles. The involved weighting factors can be chosen to minimize the variance of the free energy estimate, which leads to the minimum variance pathway (MVP). The MVP was derived independently by Blondel[51] in the context of an optimal alchemical pathway for TI, by Pham and Shirts[45] in connection with an optimized soft core pathway, and, generalized to the mean squared error for a series of intermediate states, by Reinhardt and Grubmüller.[52]

The goal of the present article is to exploit the connection between the MVP and the enveloping distribution sampling (EDS) method.[17,53,54] First, it is shown that EDS can be generalized to an improved way to generate intermediate states, which is termed λ-EDS. The Theory section demonstrates that EDS and MVP are special cases of λ-EDS, while EI is a limiting case. Moreover, λ-EDS represents a form of SCP that is able to alleviate singularity issues while avoiding the need for postprocessing. The use of λ-EDS is discussed in two parts, in order to cover the main types of free energy calculation techniques (TI as well as FEP and BAR). In the first part, the effect of λ-EDS on TI calculations is exemplified with two systems: (i) the charge inversion of an ion in a dipolar solvent, which illustrates the relationship to conventional TI intermediate states, and (ii) the creation of a cavity in a dipolar solvent, which focuses on the similarities between λ-EDS and the use of SCP. The second part compares the performance of λ-EDS with that of conventional intermediate states using the FEP and BAR free energy estimators. It also covers the optimal choice of parameters for (i) shifted harmonic oscillators, (ii) mutations of two-dimensional dihedral potentials, and (iii) cavity formation in water. Based on these results, practical advice is provided for the efficient use of λ-EDS in free energy calculations.

Theory

Free Energy Estimators

Thermodynamic integration (TI)[11,22] is one of the main techniques to estimate free energy differences. It uses the coupling parameter λ to interpolate between the Hamiltonians of the initial state $H_A = H(0)$ and the final state $H_B = H(1)$. The free energy difference is calculated as

$$\Delta G^{\mathrm{TI}}_{A\to B} = \int_0^1 \left\langle \frac{\partial H(\lambda)}{\partial \lambda} \right\rangle_\lambda d\lambda \ , \tag{1}$$

where $\langle \cdots \rangle_\lambda$ denotes an ensemble average at a particular λ-value, which is obtained in practice from MD simulations. The integral is approximated by numerical quadrature[55–58] or curve fitting.[55,56,59–61] The accuracy of the free energy estimate depends on the number and distribution of the simulated λ-points, as well as the quality of the sampling and of the numerical quadrature.

The free energy perturbation (FEP) estimator[23,28] provides the free energy difference based on a trajectory of a single state. For example,

$$\Delta G^{\mathrm{FEP}}_{A\to B} = -\beta^{-1} \ln \left\langle e^{-\beta(H_B - H_A)} \right\rangle_A \ , \tag{2}$$

where $\beta = (k_B T)^{-1}$, k_B being Boltzmann's constant and T the absolute temperature. For a series of N λ-states (including the end states $\lambda = 0$ and $\lambda = 1$), the free energy difference can be evaluated using multiple FEP steps, as

$$\Delta G^{(N-1)\times\mathrm{FEP}}_{A\to B} = \sum_{i=1}^{N-1} \Delta G^{\mathrm{FEP}}_{\lambda_i \to \lambda_{i+1}} \ . \tag{3}$$

Other free energy estimators can also be used in the sum of Eq. 3. Bennett's acceptance ratio (BAR)[29,30] provides the maximum-likelihood free energy difference given two trajectories. If simulations are only performed at the end states A and B, the free energy difference

is

$$\Delta G^{\mathrm{BAR}}_{A\to B} = -\beta^{-1} \ln \left(\frac{\langle f(V_A - V_B + C) \rangle_B}{\langle f(V_B - V_A - C) \rangle_A} \right) + C \ , \tag{4}$$

where $f(x) = (1 + e^{\beta x})^{-1}$ denotes the Fermi function, and C is determined iteratively. The efficiencies of FEP and BAR are strongly affected by the phase space overlap between the states.[7–9,62,63] Although BAR relies on two simulations while FEP needs only one, the BAR estimator is still significantly more efficient than FEP.[9,57]

Intermediate States

In the following, we consider different ways to construct the potential energy surface of intermediate states in alchemical free energy calculations. The simplest coupling scheme is energy interpolation (EI), where the hybrid potential energy $V(\lambda)$ is defined by

$$V_{\mathrm{EI}}(\lambda) = (1 - \lambda)\, V_A + \lambda\, V_B \ . \tag{5}$$

The calculation of V_{EI} requires two potential energy evaluations, one for state A and one for state B. However, the scheme is separable in λ, *i.e.,* it can be formulated as λ-dependent combination of two λ-independent terms. Once the potential energies of the end states are known, V_{EI} can be calculated for any λ-value. Notably, nonlinear schemes have also been considered.[24,25,45,64] Since EI is agnostic in regard to the type and functional form of the force field terms, it is relatively easy to implement in a simulation code. For this reason, it is used in most simulation programs. The expression TI is often used synonymously with use of EI.

The parameter interpolation (PI) scheme[10,24,25] combines the involved force field parameters $\mathbf{q}$ of the end states, *i.e.,*

$$V_{\mathrm{PI}}(\lambda) = V\left((1 - \lambda)\, \mathbf{q}_A + \lambda\, \mathbf{q}_B\right) \ . \tag{6}$$

If the parameters correspond to multiplicative prefactors, Eq. 6 is equivalent to Eq. 5. Therefore, EI and PI typically differ only for the covalent terms, which involve geometrical parameters (bond lengths, bond angles, and dihedral angles). In contrast, the nonbonded parameters (charges, Lennard-Jones C_6 and C_{12} coefficients) are multiplicative.[24] The calculation of V_{PI} requires a single potential energy evaluation with the precombined parameters, which can be generated using an external script.[26,27] However, additional potential energy evaluations are necessary for FEP or (M)BAR, as the coupling is no longer separable in λ. This problem can be addressed to some extent by using advanced methods such as λ-WHAM[65] or extended TI.[66]

The EI and PI schemes are compared in Fig. 1 (top row) for a mutation of the equilibrium bond length of a harmonic bond. The PI approach (Fig. 1a) relies on a linear combination of the equilibrium bond length $r^{eq}(\lambda) = (1-\lambda)\, r_A^{eq} + \lambda r_B^{eq}$. The EI approach (Fig. 1b) relies on a linear combination of the potential energies of states A and B according to Eq. 5. This leads to high potential energies for the intermediate states. However, their impact on the free energy difference cancels out over the pathway.

The SCP schemes[15,35,36,44–50] aim at alleviating the van der Waals endpoint problem in alchemical transformations with dummy atoms. For a pairwise nonbonded potential energy term V depending on the interparticle distance as r^{-n}, a typical SCP combination[45] reads

$$V_{\mathrm{SC}}(\lambda) = (1-\lambda)^a \epsilon_A \left[\alpha\lambda^b + (r/\sigma_A)^c\right]^{-n/c} + \lambda^a \epsilon_B \left[\alpha\,(1-\lambda)^b + (r/\sigma_B)^c\right]^{-n/c} , \qquad (7)$$

where a, b and c are positive integers, and α is a positive parameter controlling the extent of the softening (*i.e.,* the finite value of the interaction at $r = 0$). For example, a Lennard-Jones potential involves terms with $n = 6$ and $n = 12$, where σ is the collision diameter and ϵ is four times the well depth with opposite signs for the repulsive and attractive contributions. Since the SCP potential depends on both r and λ, the scheme is no longer separable in λ. Thus, the potential energy must be recalculated for the relevant other λ-points in FEP,

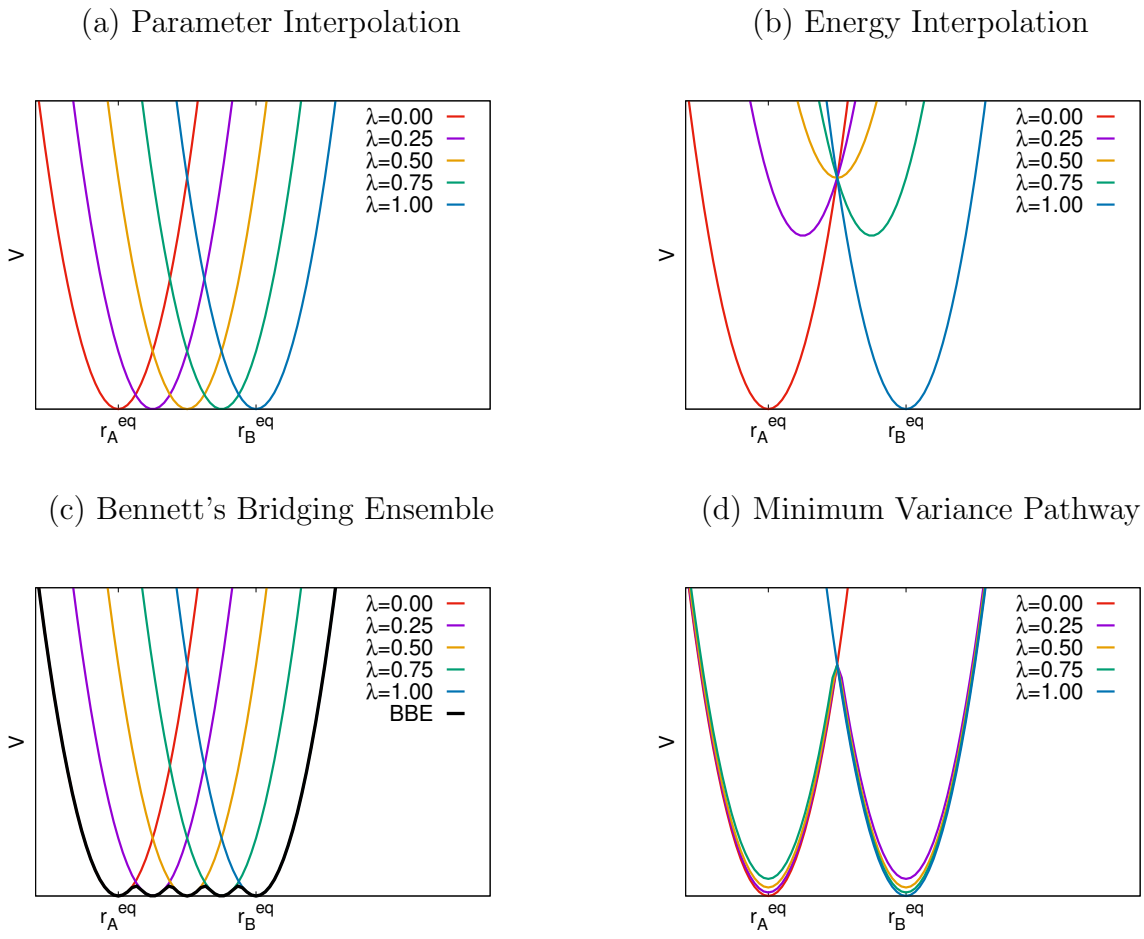

Figure 1: Potential energy functions V of intermediate states for a mutation of the equilibrium bond length r^{eq} of a harmonic bond. Four schemes are compared, namely: (a) Parameter interpolation (PI, Eq. 6); (b) Energy interpolation (EI, Eq. 5); (c) Bennett's bridging ensemble (BBE, Eq. 9); (d) Minimum variance pathway (MVP, Eq. 11). For EI, PI, and MVP, five different equispaced λ-points are are shown in different colors. $\lambda = 0$ and 1 correspond to the end states A and B, respectively. For BBE, the single intermediate state (black curve) is constructed based on a PI scheme with the five λ-values. All quantities are in arbitrary units.

BAR, or MBAR.

As can be seen in Fig. 1 (top row), both EI and PI typically require many intermediate states for bridging the phase spaces of the end states. This is due to the stiffness of the potential energy functions of the end states, which is preserved in the intermediate states. Bridging the gap with a single intermediate requires a broadening of the associated potential energy function, so that the corresponding configurational distribution can simultaneously

overlap with both end states. This idea underlies methods such as one-step perturbation with soft sites,[15,16,67–70] or enveloping distribution sampling (EDS).[17,53,54]

EDS relies on a weighted exponential average of N states, as

$$H_{\mathrm{EDS}} = -\left(\beta s\right)^{-1} \ln \left[\sum_{i=1}^{N} e^{-\beta s (H_i - E_i)} \right], \tag{8}$$

where H_i is the Hamiltonian of state i, E_i is an energy offset that compensates for a possible potential energy mismatch between the states, and s is a smoothness parameter that determines the shape of the resulting potential energy surface. This is illustrated in Fig. 2 for two harmonic oscillators with different force constants and reference lengths. In the limit $s \to \infty$, H_{EDS} follows the lower potential energy among those of the two end states. In the limit $s \to 0$, it favors a region of phase space where both states simultaneously exhibit a relatively low potential energy. Negative s-values are not used in practice, as their H_{EDS} follows the highest potential energy among the end states.

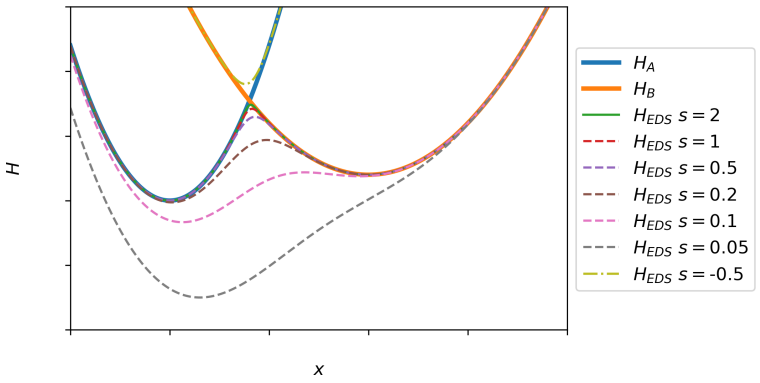

Figure 2: Hamiltonians associated with the EDS reference state for a simultaneous change of the reference length and force constant of a harmonic bond, considering different values of the smoothness parameter s. The EDS combination, defined by Eq. 8, is shown here in terms of the Hamiltonian as a function of the bond length x. The end state Hamiltonians H_A and H_B are also shown for comparison. All quantities are in arbitrary units.

Although it predates EDS by over 30 years, the BBE scheme[29] can be viewed as a form of EDS with $s = 1$ in which the N combined states are the λ-intermediates of an alchemical

transformation. This results in the expression

$$H_{\mathrm{BBE}} = -\beta^{-1} \ln \left\{ \sum_{i=1}^{N} e^{-\beta[H(\lambda_i) - E(\lambda_i)]} \right\}, \tag{9}$$

which corresponds to Eq. 25 in Ref. 29. An illustration of the BBE scheme is provided in Fig. 1c for the harmonic oscillator example with $N = 5$ equispaced states along a PI alchemical transformation. The potential energy of BBE (black curve) approximately follows the lowest potential energy among the five considered λ-states (colored curves), thus being able to sample the entire relevant phase space in one simulation.

If the selected coupling scheme is not separable in λ, the calculation of H_{BBE} requires N potential energy evaluations, which may be expensive. However, with EI, many points can be used without incurring a significant increase in computational cost. The application of BBE with EI is the basis of the integrated Hamiltonian sampling (IHS) approach.[71] In the limit $N \to \infty$, the corresponding Hamiltonian can be written as

$$H_{\mathrm{IHS}} = -\beta^{-1} \ln \left\{ \int d\lambda \, e^{-\beta[(1-\lambda)H_A + \lambda H_B - E(\lambda)]} \right\}, \tag{10}$$

where the energy offsets become a continuous function $E(\lambda)$. For large N, and provided that $E(\lambda)$ is appropriately preoptimized, IHS is expected to sample the phase space between the two end states in a continuous and largely homogeneous fashion.

The minimum variance pathway (MVP), as derived by Blondel,[51] Pham and Shirts,[45] and Reinhardt and Grubmüller,[52] can be written as

$$H_{\mathrm{MVP}}(\lambda) = -2\beta^{-1} \ln \left\{ (1-\lambda) \, e^{-\frac{\beta}{2} H_A} + \lambda \, e^{-\frac{\beta}{2}(H_B - \Delta G_{A \to B})} \right\}. \tag{11}$$

It is expected to provide the lowest possible variance in the calculated free energy, but requires an estimate of the free energy difference between the end states ($\Delta G_{A \to B}$), analogously to the energy offset in EDS. The main issue with the MVP scheme is that it tends to generate

high energy barriers.[4,6,72,73] This can make the MVP method very inefficient in practice.[45,51] An illustration of the MVP scheme is provided in Fig. 1d, considering the harmonic oscillator example and five equispaced λ-values. For λ-values of 0 and 1, the end states are recovered. However, for the three intermediate λ-values, the potential energy curves present a high barrier along the conformational coordinate, so that the system remains trapped in the starting energy well. Thus, even if the variance of the free energy estimate is low, the result is incorrect and exhibits large hysteresis.

The λ-EDS Scheme

In its most general form, the proposed λ-EDS scheme reads

$$H_{\lambda-\mathrm{EDS}}(\lambda) = -\left[\beta s(\lambda)\right]^{-1} \ln\left\{(1-\lambda)\, e^{-\beta s(\lambda) H_A} + \lambda\, e^{-\beta s(\lambda)\,[H_B - E(\lambda)]}\right\} \ , \tag{12}$$

where both $s(\lambda)$ and $E(\lambda)$ evolve along the alchemical pathway. Except for a constant, the above equation encompasses EDS as a special case at $\lambda = 0.5$, and MVP as a special case with $s = 0.5$ and $E = \Delta G$. In other words, λ-EDS is identical with the MVP except for the introduction of an additional variable s, and simply adds a λ-dependence to conventional EDS. With $s = 1$, it is equivalent to BBE based on the two end states. Notably, only energy evaluations at the end states are required, which means that λ-EDS is separable in λ. In the following, we refer to intermediate states that were generated with λ-EDS at a λ-value of x as λ-EDS(x). For example, the initial state of the alchemical transformation at $\lambda = 0.0$ is referred to as λ-EDS(0.0). Note that the midpoint of the alchemical pathway at λ-EDS(0.5) is equivalent to the original EDS. We will, however, keep using the term λ-EDS(0.5) in the following simply to ensure a consistent nomenclature throughout the publication.

Relationship Between λ-EDS and TI

For TI, the λ-derivative of $H_{\lambda-\mathrm{EDS}}$ with constant values of s and E is given by

$$\frac{\partial H_{\lambda-\mathrm{EDS}}(\lambda)}{\partial \lambda} = \frac{e^{-\beta s(H_B-E)} - e^{-\beta s H_A}}{\beta s \left[(1-\lambda)\, e^{-\beta s H_A} + \lambda\, e^{-\beta s(H_B-E)}\right]} \,, \tag{13}$$

where all the involved exponential terms are already available from the calculation of $H_{\lambda-\mathrm{EDS}}$. The application of TI using Eq. 13 leads to $\Delta G_{A\to B} - E$, *i.e.,* the result must be increased by E.

In the limit of $s \to 0$, Eq. 12 becomes,

$$\lim_{s\to 0} H_{\lambda-EDS}(\lambda) = (1-\lambda)\, H_A + \lambda\, (H_B - E)\,, \tag{14}$$

which, apart from the inclusion of the energy offset E, is identical to conventional EI in Eq. 5. This result is illustrated in Fig. 3 for two harmonic oscillators with shifted potential energy minima and different force constants. For conventional EI (Fig. 3a), the potential energy map has a single minimum at all λ-values. The valley is slightly curved due to the different force constants of the end states. In contrast, for λ-EDS with $s = 0.5$ (Fig. 3b), which is equivalent to MVP, the map presents two valleys that are separated by high energy barriers. As the s-value is reduced to 0.125 (Fig. 3c), the crest between the two energy valleys becomes closer to a saddle-point. For an s-value of 0.01 (Fig. 3d), the potential energy surface of λ-EDS resembles very closely the one of conventional TI with EI.

In the limiting case where H_B is singular, Eq. 13 becomes

$$\lim_{H_B\to\infty} \frac{\partial H_{\lambda-EDS}(\lambda)}{\partial \lambda} = \frac{1}{(1-\lambda)\beta s} \,. \tag{15}$$

Thus, the derivative of the λ-EDS Hamiltonian remains finite. Given an appropriate choice for s, the λ-EDS scheme can solve the van der Waals endpoint problem just as well as the traditional SCP approaches. In addition, λ-EDS remains separable in λ, which means that

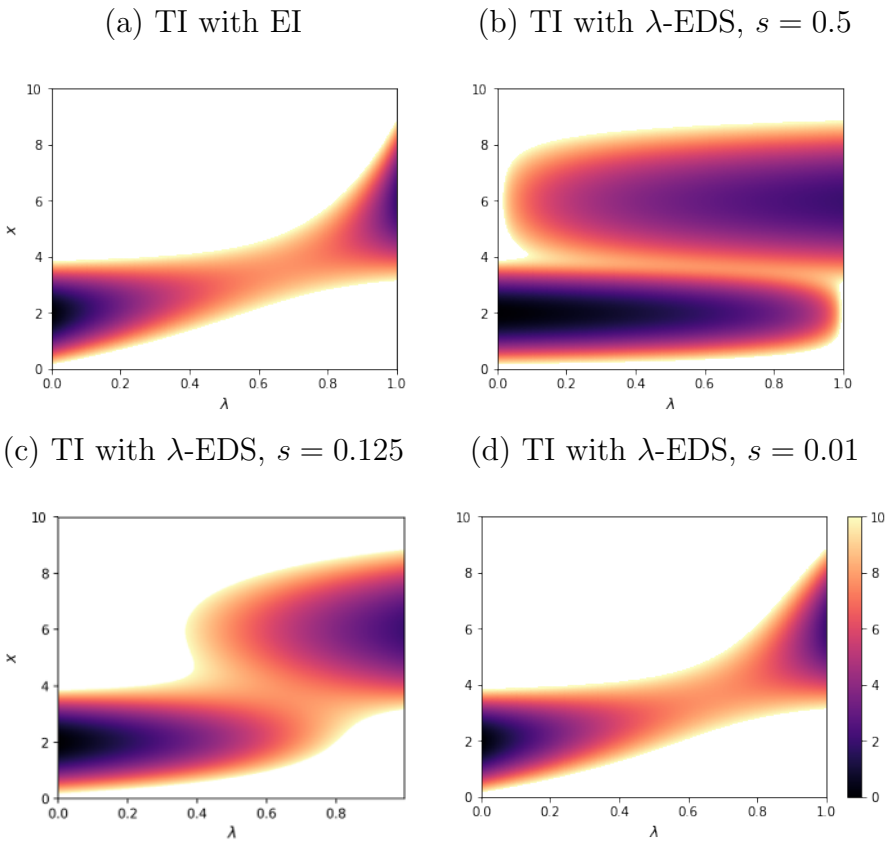

Figure 3: Potential energy functions associated with (a) conventional TI based on EI, compared to λ-EDS with different choices of s, *i.e.,* (b) $s = 0.5$,(c) $s = 0.125$, and (d) $s = 0.01$, for a simultaneous change of the equilibrium bond length and force constant of a harmonic oscillator. The quantities λ, x and V are the coupling parameter, the bond length, and the potential energy, respectively. All quantities are in arbitrary units.

there is no computational overhead when using FEP or (M)BAR. The similarity between λ-EDS and SCP is illustrated in Fig. 4 for the Lennard-Jones (LJ) interaction of two particles where a dummy atom (state A) is turned into a LJ particle (state B). The normal LJ potential of state B (thick blue curve) leads to an infinite interaction energy as the inter-particle distance r decreases to zero. For the lowest s-value of 0.01 (violet curve in Fig. 4a), the λ-EDS(0.5) interaction is nearly equivalent to that of TI with EI at $\lambda = 0.5$ (dashed red curve in Fig. 4a). For such low s-values, the potential energy of state B contributes significantly, which leads to a hard potential. For higher s-values (three other colored curves in Fig. 4a), the energy is dominated by the dummy atom state A, which results in a finite and

nearly constant repulsion at short distances. The smoothness parameter s modulates the finite value at zero distance in a similar way as the softness parameter α in a conventional SCP scheme (Fig. 4b), except that λ-EDS(0.5) maintains slightly more phase space overlap with the LJ particle in state B. However, almost identical curves can be obtained for EDS and SCP when using Eq. 7 with the recommended c-value of 48 from Ref. 44 and very low α-values.

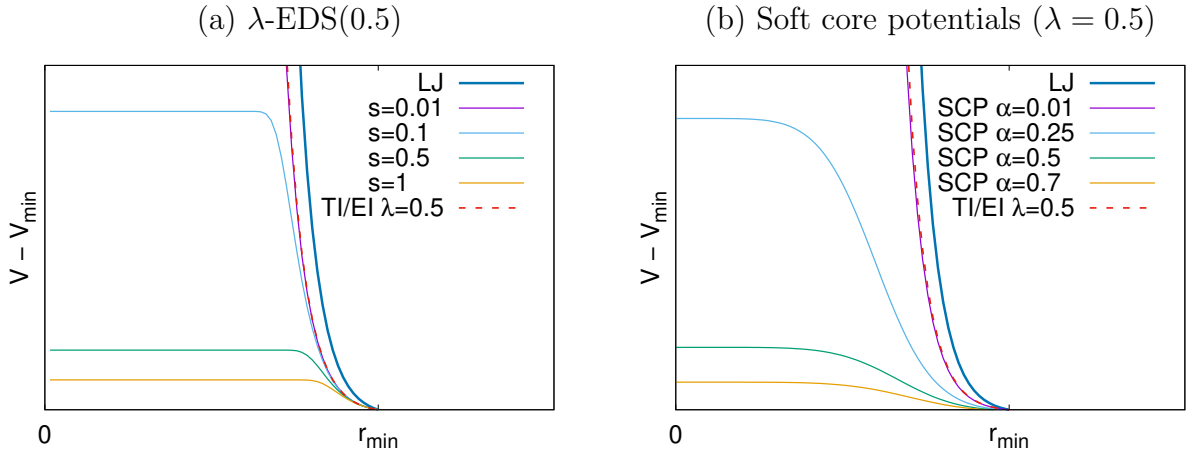

Figure 4: Potential energy functions associated with intermediate states along the λ-dependent change involving a LJ test particle interacting with a dummy particle (state A) or with another LJ particle (state B). The physical LJ energy (thick blue curve) is shown along with TI based on EI for $\lambda = 0.5$ (dashed red curve). (a) λ-EDS(0.5) at different values of s is compared to (b) SCP based on Eq. 7 with different α-parameters, along with $\lambda = 0.5$, $a = 1$, $b = 2$, and $c = 6$ (solid colored curves). The quantities r and $V - V_{\text{min}}$ are the interparticle distance and the potential energy relative to the energy minimum V_{min}, respectively. All quantities are in arbitrary units.

Estimating Appropriate s-Values

The MVP is expected to be the optimal pathway in terms of efficiency given a simulation that samples the entire phase space. However, if the simulation suffers from sampling problems, the MVP leads to biased results. In such cases, the s-value in λ-EDS(0.5) needs to be adjusted. An adaptive approach to find an appropriate s-value based on an estimate of the free energy difference between the states was proposed by Christ and van Gunsteren.[53] This

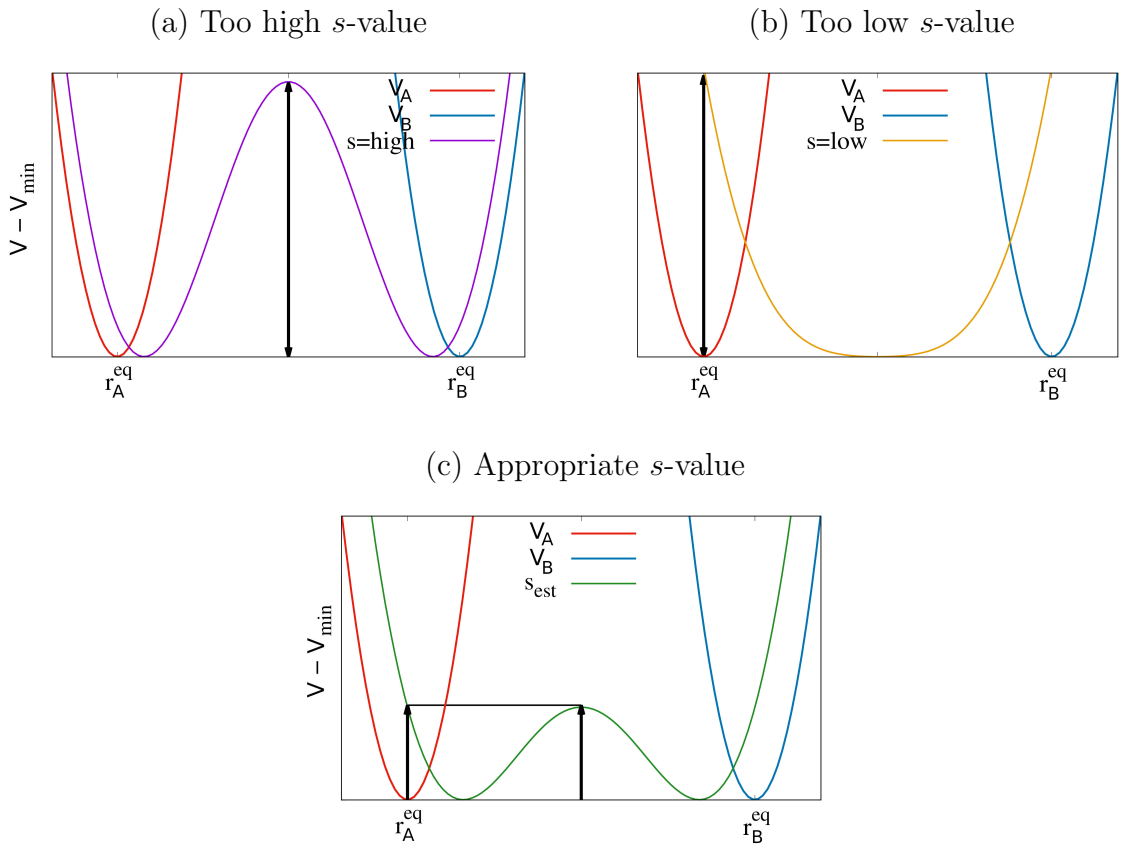

Figure 5: Three different scenarios for the choice of the s-value in λ-EDS(0.5), illustrated for mutations of the equilibrium bond length of a harmonic bond. The panels refer to s-values that are: (a) too low; (b) too high; (c) appropriate. The quantities r and V are the bond length and the potential energy, respectively. All quantities are in arbitrary units.

scheme attempts to reduce the energy barrier between the states within the EDS potential to $k_{\mathrm{B}}T$. However, it tends to underestimate the s-values for large energy offsets.[74] This indicates that finding a good s-value to optimize the sampling and convergence of relatively short λ-EDS simulations requires other factors than just free energy differences between the end states. To address this problem, advanced techniques such as or replica exchange EDS (RE-EDS),[75,76] which employs several s-values to circumvent the energy barriers, or accelerated EDS,[77] which reduces the energy barriers, have been introduced. The fundamental problem in choosing the s-value is illustrated in Fig. 5 for λ-EDS of two shifted harmonic oscillators with a free energy difference of zero. Here, the optimal s-value is related to the alchemical energy barrier $\Delta V_{barrier}$ at the intersection between the potential energy curves of the end

states. If s is too high (Fig. 5a), the energy barrier remains high, which impairs sampling. If s is too low (Fig. 5b), λ-EDS will closely resemble EI at $\lambda = 0.5$. This reduces the phase space overlap with the end states, which has a detrimental effect on the convergence of the free energy calculation. As illustrated in Fig. 5c, a possible compromise involves the choice of an s-value for which the energy levels at the energy barrier and at the minima of the end states have comparable magnitudes. In a linear response formalism,[9,78,79] this constraint can be solved for s (one real solution) with an estimated s_{est} given by

$$s_{\mathrm{est}} = \frac{1}{\beta \Delta V_{barrier}} \ln \left[\frac{1 + \left(19 - 3\sqrt{33}\right)^{\frac{1}{3}} + \left(19 + 3\sqrt{33}\right)^{\frac{1}{3}}}{3} \right] \approx \frac{0.609}{\beta \Delta V_{barrier}} \, . \qquad (16)$$

For changes of covalent terms or umbrella sampling, $\Delta V_{barrier}$ can be directly determined from the force constants and the step size. However, Eq. 16 does not require an explicit knowledge of the equilibrium positions or force constants of the harmonic potential energy wells in states A and B, as only the resulting $\Delta V_{barrier}$ is relevant. For simple transformations of covalent terms or of the charge of monoatomic ions in solution, $\Delta V_{barrier}$ can be guessed by performing two energy minimizations. The first energy minimization aims at the global energy minimum with EI at $\lambda = 0.5$. The resulting structure can then be minimized again using the potential energy function of either state A or state B. The value of $\Delta V_{barrier}$ corresponds to the decrease in potential energy occurring during this second energy minimization. For more complex systems, a series of structures from the equilibration stage can be employed to estimate the average $\Delta V_{barrier}$. An analogous linear response approach was used previously to successfully estimate the variance of free energy estimates.[9] However, the method fails if dummy atoms or large changes of force constants are involved.

Methods

The λ-EDS scheme is first used for TI calculations of two benchmark systems: (*i*) the charge inversion of an ion in a dipolar solvent, to illustrate the relationship with EI; (*ii*) the formation of a LJ cavity in a dipolar solvent, to illustrate the relationship to SCP. Three benchmark systems serve to compare the efficiencies of conventional intermediate states and λ-EDS in connection with the BAR and FEP estimators: (a) shifted harmonic oscillators; (b) two-dimensional dihedral potentials; (c) cavity creation in water. For the simple benchmark systems in the present study, $s(\lambda)$ is chosen to be λ-independent and $E(\lambda) = 0$.

Charge Inversion

The MD simulations were performed with a modified version of the GROMOS program.[80–82] They involved cubic computational boxes containing 750 dipolar solvent molecules and one solute, simulated under periodic boundary conditions in the isothermal-isobaric ensemble. The solvent molecules consist of two isosteric atoms with partial charges of -0.8 and $+0.8$ e, and square-root LJ interaction parameters $C_6^{1/2} = 0.057903$ $(\,\mathrm{kJ\,mol^{-1}}\,)^{\frac{1}{2}}\,\mathrm{nm^3}$ and $C_{12}^{1/2} = 1.9877 \cdot 10^{-3}$ $(\,\mathrm{kJ\,mol^{-1}}\,)^{\frac{1}{2}}\,\mathrm{nm^6}$. The solute is a charged cavity corresponding to a chloride ion, with interaction parameters $C_6^{1/2} = 0.1175$ $(\,\mathrm{kJ\,mol^{-1}}\,)^{\frac{1}{2}}\,\mathrm{nm^3}$ and $C_{12}^{1/2} = 1.034 \cdot 10^{-2}$ $(\,\mathrm{kJ\,mol^{-1}}\,)^{\frac{1}{2}}\,\mathrm{nm^6}$. Newton's equations of motion were integrated with a timestep of 2 fs. The temperature was maintained at 298.15 K using a weak-coupling thermostat[83] with a relaxation time of 0.1 ps. The pressure was kept close to 1 bar using a weak-coupling barostat[83] with a relaxation time of 0.5 ps and an isothermal compressibility of $1.71 \cdot 10^{-3}$ $(\mathrm{kJ\,mol^{-1}\,nm^{-3}})^{-1}$. Reaction-field electrostatics were used with a solvent dielectric permittivity of 52.4. The TI simulations involved 1 ns of production after 0.1 ns of equilibration at each λ-point. The Hamiltonian derivatives were saved every timestep. Numerical integration was performed with Simpson's quadrature,[56–58] also known as Kepler's wine barrel method.[84]

The charge of the solute was changed from -1 to $+1\,e$. The TI calculations relied on 11 equidistant λ-points in the range [0,1]. The free energy changes of λ-EDS with different s-values are compared to the results of TI calculations with the EI scheme. The analytical reference result is zero. The error bars correspond to 95% confidence intervals based on an autocorrelation analysis. To detect hysteresis, two seeding schemes for the initial configurations were considered,[6] namely left seeding (starting from $\lambda = 0$ and proceeding to $\lambda = 1$) and right seeding (from $\lambda = 1$ to $\lambda = 0$). Each simulation was equilibrated for 0.1 ns starting from the equilibrated structure of the previous (left seeding) or next (right seeding) λ-point.

Cavity Creation with λ-EDS

The cavity-formation benchmark involves a change from a dummy site to a neutral chloride-sized LJ cavity within the dipolar solvent. The TI calculation relied on 11 equidistant λ-points in the range [0,1], plus up to 16 additional λ-points in ranges with high curvature. The free energy estimates from λ-EDS with different s-values are compared to TI calculations with SCP acting on both the dispersive and the repulsive components of the LJ interaction, using $a = 1$, $b = 2$, and $c = 6$ based on Eq. 7 (following Ref. 35) along with $\lambda = 0.5$ and soft core parameters α of 0.1, 0.2, and 0.5. Here, the seeding scheme relies on 0.1 ns equilibration at the given λ-point, starting from a common configuration that was equilibrated with SCP at $\lambda = 1$.

Shifted Harmonic Oscillators

Gas phase simulations were performed for a linear four-atomic molecule with atomic masses of $1\,\mathrm{g\,mol^{-1}}$, and without nonbonded interactions. In the initial state A, all harmonic bond stretching potentials have equilibrium bond lengths of 0.2 nm and force constants of $8.4 \cdot 10^4\,\mathrm{kJ\,mol^{-1}\ nm^{-2}}$. The harmonic bond angle bending potentials have equilibrium angles of 113.6° and force constants of $209.2\,\mathrm{kJ\,mol^{-1}\ rad^{-2}}$, and the dihedral potential has a multiplicity of three, a phase shift of 180°, and a force constant of $4.187\ \mathrm{kJ\,mol^{-1}}$. A series

of final states B is considered, in which the equilibrium bond length at the last atom is changed from 0.2 nm to values between 0.215 and 0.250 nm in steps of 0.05 nm.

The simulations were carried out with CHARMM,[85,86] using the EDS implementation[87–90] of the MSCALE module.[91] For each state, Langevin's equation of motion was integrated over 1 ns with a timestep of 1 fs using a friction coefficient of 1 ps^{-1} and random forces appropriate for a temperature of 300 K. Trajectories were written every 1000 steps, and the free energy analysis was performed with the FREN module[9,92] of CHARMM. To estimate error bars, each free energy simulation was repeated ten times using different initial velocities. The FEP results calculated from simulations with λ-EDS(0.5) are compared to the results of FEP based on state A, as well as BAR based on states A and B. The analytical reference result arises from a Jacobian term.[93–97]

Shifted Two-dimensional Dihedral Potentials

Gas phase simulations were performed for a linear five-atomic molecule without nonbonded interactions. The bonds and angles are constrained and the potential energy is determined by the dihedral angles ϕ and ψ as

$$V(\phi,\psi) = \frac{K}{2}\left[\cos(n\phi-\delta)+\cos(n\psi-\delta)\right], \tag{17}$$

where K is the force constant, $n = 2$ is the multiplicity, and δ corresponds to a phase shift. In end states A and B, the phase shifts are set to $\delta_A = 0°$ and $\delta_B = 180°$, respectively. Thus, the four energy minima of one end state coincide with the four energy maxima of the other end state. The free energy difference is zero by symmetry, but the phase space overlap between the two states is very small, inducing severe sampling problems.

The sampling was performed within the Ensembler package[98] using the Metropolis Monte Carlo algorithm[99] with random steps of $-1°$ or $+1°$ for both ϕ and ψ. Three force constants of 5, 20, and 50 k_BT at an arbitrary temperature were considered, along with λ-EDS(0.5) at s-

values of 1, 0.5, 0.1, 0.01, and s_{est} from of Eq. 16. Here, $\Delta V_{barrier}$ is equal to the force constant K. One calculation was also carried out with the replica exchange EDS approach,[75,76] in which EDS is combined with Hamiltonian replica exchange.[100–102] Exchanges were attempted between two replicas ($s = 0.5$ and 0.01) every 1000 steps. The sampling involved 1 million steps, and the calculations were repeated ten times with different random seeds to estimate error bars.

Lennard-Jones Particle in Water

The last benchmark system considers the creation of a LJ particle in water. The solute is a dummy atom (state A), or a series of uncharged LJ particles with a well depth ϵ of $-0.041\,\text{kJ}\,\text{mol}^{-1}$ and radii S ranging from 0.05 nm to 0.40 nm in steps of 0.05 nm (states B). The effective radius S is one half of the collision diameter σ for the interaction between the solute and water, based on an arithmetic-mean combination rule for the homoatomic parameters.

The simulations were carried out with CHARMM,[85,86] using the EDS implementation[87–90] of the MSCALE module.[91] They involved a cubic computational box containing 1291 TIP3P water molecules[103] and one solute, simulated under periodic boundary conditions in the canonical ensemble. The box volume was set based on 0.5 ns of preequilibration at a constant pressure of 1 bar, resulting in edge lengths of about 3.4 nm. The temperature was maintained at 300 K using a Nosé-Hoover thermostat[104,105] with a temperature piston mass of 19455.6 $\text{kJ}\,\text{mol}^{-1}$ ps^2. The SHAKE algorithm[106] was used to keep the water molecules rigid.

The nonbonded interactions were truncated at 1.2 nm using force shifting for the electrostatic interactions and potential shifting for the LJ interactions.[107] The timestep was 1 fs and trajectories were written every 100 steps. The simulations lasted 2 ns after 0.5 ns equilibration at constant volume, and were repeated ten times with different initial velocities to estimate error bars. The FEP results of λ-EDS(0.5) with s-values of 1.0, 0.5, 0.1, and

0.01 are compared to the results of FEP based on state B, and BAR based on states A and B. The SCP simulations were conducted with the PERT module, using the PSSP keyword. The accurate reference calculations relied on a variant of serial insertion[26] with 69 different values of the radius S ranging from 0.0 to 0.45 nm.

Results and Discussion

Charge Inversion Using TI with EI and λ-EDS

The average λ-derivatives of the Hamiltonian in TI calculations of the charge inversion of a chloride ion in a perfectly dipolar solvent are shown in Fig. 6, considering EI and λ-EDS. The results obtained with left or right seeding are shown separately (blue solid and orange dotted curves, respectively). The corresponding free energy differences are reported in Table 1.

Irrespective of the seeding, the EI calculations (Fig. 6a) yield nearly straight lines, as expected from the linear response of dipolar solvents to limited charge changes. The resulting free energy differences are 0.2 ± 1.8 and $0.2 \pm 1.5\,\mathrm{kJ\,mol^{-1}}$ for left and right seeding, which agrees with the analytical result of zero. The absence of hysteresis is a result of the linear λ-dependent charge evolution from -1 to $+1\,e$ with EI. Here, the solvent can relax within picoseconds to any charge change, and is not affected by any significant energy barriers.

The situation is very different for the MVP (Fig. 6b), where the two seeding directions yield distinct curves. The resulting free energy differences are $15.3 \pm 0.0\,\mathrm{kJ\,mol^{-1}}$ and $-15.3 \pm 0.0\,\mathrm{kJ\,mol^{-1}}$ for left and right seeding, respectively. The results are more precise than TI with EI, but entirely incorrect. The hysteresis arises because MVP combines the potential energy minima of both the negative and the positive ion. At the midpoint of the transformation, solvent dipoles pointing towards the ion and away from ion are equally favorable, but the interconvertion with dipoles pointing sideways is energetically strongly disfavored. This is analogous to the shifted harmonic oscillators in Fig. 1d. Left seeding only samples the low energy regions of state A up to $\lambda = 0.9$, although such conformations become unfavorable

after $\lambda = 0.5$. The Hamiltonian λ-derivative is systematically too positive along the path. Only at $\lambda = 1$ does one obtain the correct energy minimum of state B. As $s \to 0$ (Fig. 6c), λ-EDS approaches the behavior of EI. Thus, adapting the s-value in λ-EDS provides the flexibility that is required to overcome the sampling problems of the MVP.

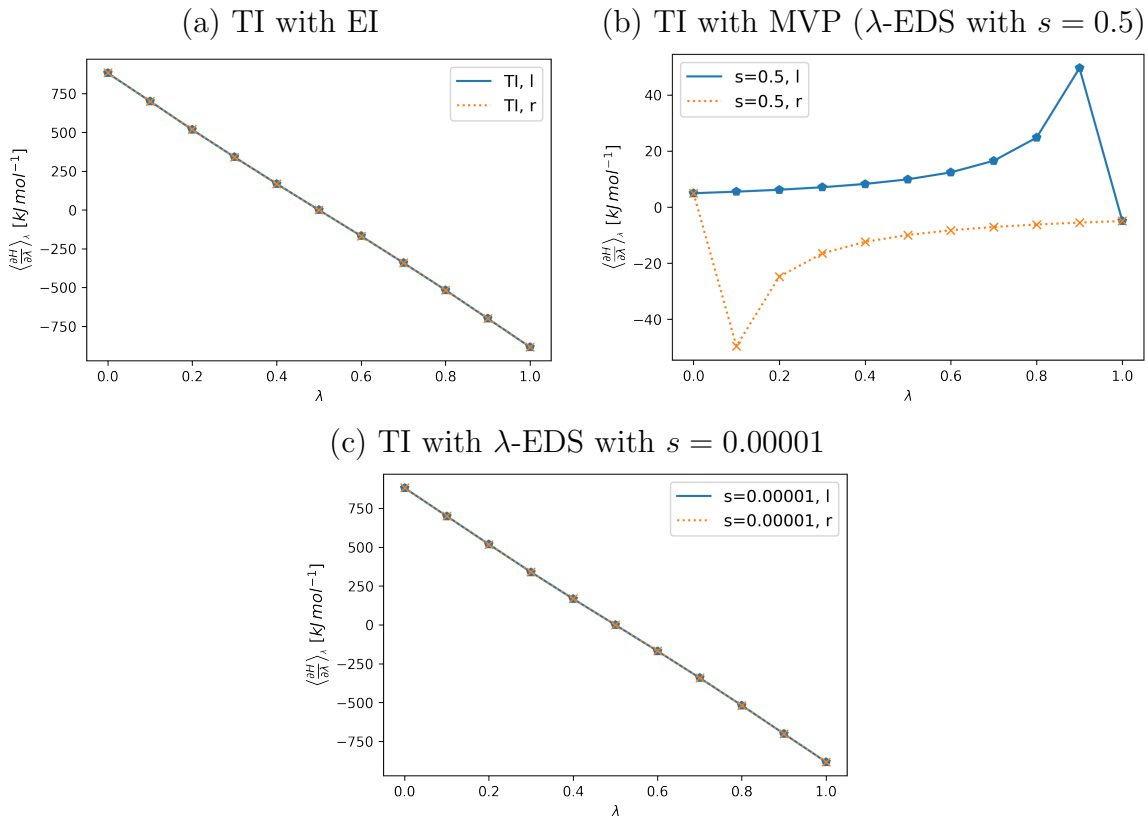

Figure 6: Average λ-derivative of the Hamiltonian in TI calculations of the charge inversion of a chloride ion in a perfectly dipolar solvent. The three graphs correspond to TI with: (a) Conventional EI; (b) MVP (λ-EDS with $s = 0.5$); (c) λ-EDS with $s = 0.00001$. The results are reported for simulations with left (l, blue curves) and right (r, orange curves) seeding to detect hysteresis.

The trend towards higher accuracy but lower precision as s decreases is clearly visible in Table 1. By lowering s to 0.005, 0.001 and 0.00001, the hysteresis is reduced to 0.9, 0.8, and 0.3 kJ mol^{-1}, respectively. However, the average error bars over the two seeding schemes increase to 0.8, 1.4, and 1.6 kJ mol^{-1}. The s-value with the optimal balance between precision and accuracy for this benchmark system is expected to reside between 0.001 and 0.01.

Table 1: Free energy differences for the charge inversion of a chloride ion in a perfectly dipolar solvent. The results are reported for EI; MVP (λ-EDS with $s = 0.5$); and λ-EDS with four other s-values, using simulations with left (ΔG_l) and right (ΔG_r) seeding, along with their absolute difference as a measure for the hysteresis. All values are in $\mathrm{kJ\,mol^{-1}}$.

Scheme	ΔG_l	ΔG_r	$\lvert \Delta G_\mathrm{l} - \Delta G_\mathrm{r} \rvert$
EI	0.2 ± 1.8	0.2 ± 1.5	0.0
λ-EDS, $s = 0.5$ (MVP)	15.3 ± 0.0	-15.3 ± 0.0	30.5
λ-EDS, $s = 0.01$	61.1 ± 0.1	-61.0 ± 0.1	122.1
λ-EDS, $s = 0.005$	0.9 ± 0.8	-0.1 ± 0.8	0.9
λ-EDS, $s = 0.001$	0.5 ± 1.4	-0.4 ± 1.3	0.8
λ-EDS, $s = 0.00001$	-0.4 ± 1.7	-0.1 ± 1.4	0.3

Cavity Creation Using TI with SCP and λ-EDS

The average λ-derivatives of the Hamiltonian in TI calculations of a cavity creation process in a perfectly dipolar solvent are shown in Fig. 7. Calculations relying on SCP with $\alpha = 0.1$ (red curve, Fig. 7a) lead to a sharp but finite peak close to $\lambda = 0$, corresponding to a relatively hard potential. Increasing α to 0.2 (orange curve) results in a softer repulsion and the peak decreases, broadens, and shifts slightly to the right. The commonly used[35] value $\alpha = 0.5$ (blue curve), corresponds to an even softer state. The calculated free energy differences are reported in Table 2, and vary between 21.6 and 22.2 $\mathrm{kJ\,mol^{-1}}$ for the different α values, which reflects the quadrature and statistical errors.

The calculations with λ-EDS (Fig. 7b) show that singularities can also be avoided with a suitable choice of s, as the λ-derivative is bounded according to Eq. 15. For $s = 0.005$ (red curve), the contribution of state B is large, which leads to a sharp peak at $\lambda = 0$ with a value of about $500\,\mathrm{kJ\,mol^{-1}}$ (in excellent agreement with the estimate from Eq. 15, see rightmost column of Table 2). The curve closely resembles the curve for SCP with $\alpha = 0.1$. Increasing s to 0.01 (orange curve) resembles a softer potential, which is similar to the curve for SCP with $\alpha = 0.2$. For $s = 0.02$ (blue curve), the contribution of state B is largely reduced, which leads to a further decrease and broadening of the peak. In contrast to the curve for SCP with $\alpha = 0.5$, the curve for λ-EDS describes a plateau-like trend at short distances instead of decreasing towards zero. The relative ease of integrating the peak-like curves of

SCP versus the plateau-like shape of λ-EDS depends on the number and placement of the λ-points, as well as the numerical quadrature scheme. However, both methods are equally capable of maintaining a finite λ-derivative of the Hamiltonian. The calculated free energy differences are reported in Table 2, and vary between 21.9 and 23.5 kJ mol^{-1} for the different s-values. Considering potential errors from sampling and numerical quadrature, the results are consistent with each other as well as with the SCP results.

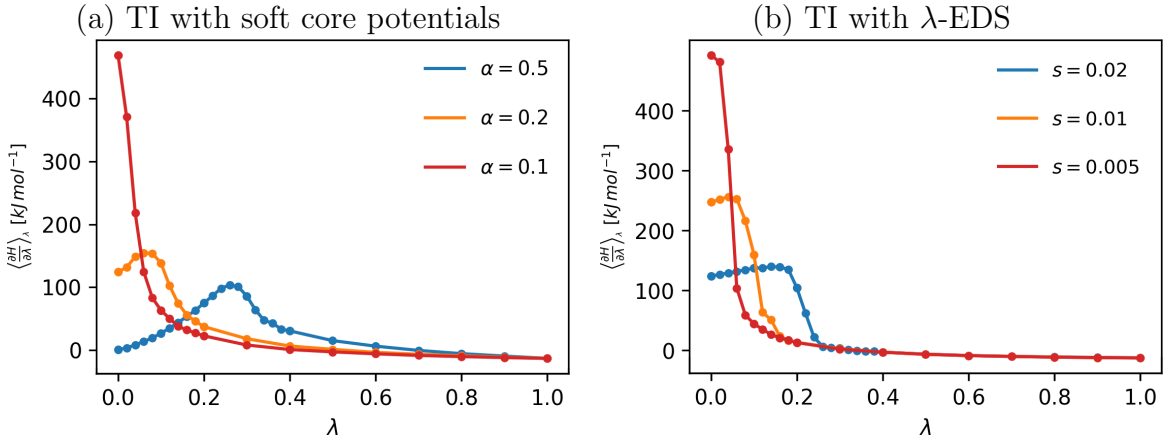

Figure 7: Average λ-derivative of the Hamiltonian in TI calculations of cavity creation in a perfectly dipolar solvent. The two graphs correspond to TI with (a) SCP using three different values of the soft core parameter α; (b) λ-EDS using three different values of the smoothness parameter s.

Table 2: Free energy change for cavity creation in a perfectly dipolar solvent. The results are reported for SCP with different α-values, and λ-EDS with different s-values. The bound of the λ-derivative of the λ-EDS-Hamiltonian according to Eq. 15 is also reported (Deriv.). All values are in kJ mol^{-1}.

Scheme	ΔG	Deriv.
SCP $\alpha = 0.1$	22.2 ± 0.5	
SCP $\alpha = 0.2$	22.2 ± 0.5	
SCP $\alpha = 0.5$	21.6 ± 0.5	
λ-EDS, $s = 0.005$	21.9 ± 0.4	495.8
λ-EDS, $s = 0.01$	23.4 ± 0.4	247.9
λ-EDS, $s = 0.02$	23.6 ± 0.3	124.0

Shifted Harmonic Oscillators

The shifted harmonic oscillator benchmark serves to test the capability of intermediate states to bridge the phase space between two energy wells. This situation is encountered in relative free energy calculations involving bond length, or bond angle changes, or when using umbrella sampling with a harmonic restraint potential.[32] It also helps to understand the previous benchmark system involving the structural rearrangement of dipoles during the charge inversion of an ion in a dipolar solvent, as both exhibit shifted Gaussian probability distributions.[79] Thus, the observations made in this section are generally relevant to free energy protocols involving changes of point charges in aqueous solution, or for constant-pH simulations.[88–90]

The average errors of different bond length mutations Δr in a hypothetical molecule are reported in Table 3. The corresponding standard deviations over ten repetitions are shown in Fig. 8 for a subset of approaches. Small errors and standard deviations for large Δr-values indicate efficient free energy schemes. Accurate results with absolute errors below $0.5\,k_\mathrm{B}T$ are shown in boldface, and precise results with standard deviations below $0.5\,k_\mathrm{B}T$ are underlined.

FEP based on a single simulation of state A leads to inaccurate and imprecise results in all cases, with errors ranging from 0.8 to $46.1\,k_\mathrm{B}T$. Because the harmonic bond is very stiff, most of the sampling is performed close to the initial equilibrium bond length, leading to very large potential energy differences relative to state B.

Combining data from states A and B with BAR leads to accurate and precise results up to Δr of 0.025 nm. Beyond this, the phase space overlap between the two end states is too limited, and the BAR method fails to converge. Although BAR calculations require twice as much computational effort as FEP, the BAR estimator is still by far more efficient. This is also evidenced by a number of previous studies.[57,62,108–111]

λ-EDS(0.5) simulations with $s = 1$, which is equivalent to BBE based on the two end states, lead to accurate results up to a Δr of 0.035 nm. This bond length change corresponds

to a mutation of a carbon-carbon bond to a carbon-sulfur bond in one step.[112] Thus, λ-EDS with $s = 1$ outperforms the use of two conventional simulations with the BAR estimator in terms of both accuracy and computational cost. Using λ-EDS(0.5) with $s = 0.5$, which corresponds to MVP, leads to a similar performance. The simulations with $s = 0.1$ performs best among all simulations with fixed s-values, as it provides accurate and precise results up to a bond length change of 0.04 nm. Further lowering the s-value to $s = 0.01$ or 0.001 diminishes the performance, giving reliable results only up to 0.025 nm. The latter simulations sample the phase space between the two end states, but lack phase space overlap (Fig. 5). Using the Δr-dependent s_{est} value from Eq. 16 leads to the best results. The required value of $\Delta V_{barrier}$ for Eq. 16 was calculated from an energy minimization of the optimized initial structure at $\lambda = 0.5$ of the EI transformation using the Hamiltonian of the initial state. The free energy results based on s_{est} remain accurate and precise up to a bond length increase of 0.05 nm. This illustrates that the optimal choice of the s-value depends on Δr. Small bond length changes can be achieved with high s-values, while large changes require lower s-values. However, too low s-values are also detrimental to the performance. If the bond length change exceeds ca. 0.05 nm, the introduction of additional λ-EDS intermediate states most likely becomes necessary.

Mutation of a Two-dimensional Dihedral Potential

The mutation of a two-dimensional dihedral potential[63,113] mimics the effect of point mutations on the rotational substates of amino acid side chains, or of a cis-trans isomerization in the protein backbone. Such mutations often involve energy barriers on the order of 10 to 25 $k_{\text{B}}T$, leading to poor convergence in conventional free energy calculations. This problem is normally addressed by enhanced sampling techniques,[87] but it can also be circumvented with specific free energy methods.[6]

The sampling afforded by λ-EDS(0.5) for the mutation of a two-dimensional dihedral potential is illustrated in Fig. 9. Here, end states A and B correspond to opposite phase

Table 3: Average errors of free energy differences associated with changes Δr of the equilibrium bond length in a hypothetical molecule. Errors relative to analytical results are reported for: (a) FEP based on simulations of state A; (b) BAR based on simulations of states A and B; (c) λ-EDS(0.5) simulations with FEP and $s = 1$, 0.5, 0.1, 0.01, 0.001, and s_{est} according to Eq. 16 (*i.e.*, $s_{\text{est}} = 0.321$, 0.181, 0.116, 0.080, 0.059, 0.045, 0.036, and 0.029 for the increasing Δr values). N_{sim} indicates the required number of simulations. Accurate results (absolute errors below $0.5\,k_{\text{B}}T$) are highlighted in boldface, while precise results (standard deviations below $0.5\,k_{\text{B}}T$) are underlined. Situations where BAR did not converge within 500 iterations are indicated by crosses. All values are in $k_{\text{B}}T$.

		Δr [nm]							
Scheme	N_{sim}	0.015	0.020	0.025	0.030	0.035	0.040	0.045	0.050
FEP from state A	1	0.8	2.5	5.8	10.5	17.0	25.0	34.7	46.1
BAR from states A and B	2	**0.0**	**0.0**	**0.0**	**0.3**	×	×	×	×
BBE (λ-EDS(0.5), $s = 1$)	1	**0.0**	**0.0**	**0.0**	**0.1**	**0.1**	16.1	32.6	44.0
MVP (λ-EDS(0.5), $s = 0.5$)	1	**0.0**	**0.1**	**0.1**	**−0.3**	**0.1**	13.7	31.4	41.9
λ-EDS(0.5), $s = 0.1$	1	**0.0**	**0.0**	**0.0**	**0.0**	**0.0**	**−0.1**	**0.1**	28.6
λ-EDS(0.5), $s = 0.01$	1	**0.0**	**−0.1**	**−0.1**	**−0.2**	**0.0**	**0.1**	**−0.4**	**−0.4**
λ-EDS(0.5), $s = 0.001$	1	**−0.1**	**0.1**	**−0.2**	**0.2**	0.7	−1.1	0.6	−0.5
λ-EDS(0.5), s_{est}	1	**0.0**	**0.0**	**0.0**	**0.0**	**0.0**	**0.0**	**0.0**	**0.0**

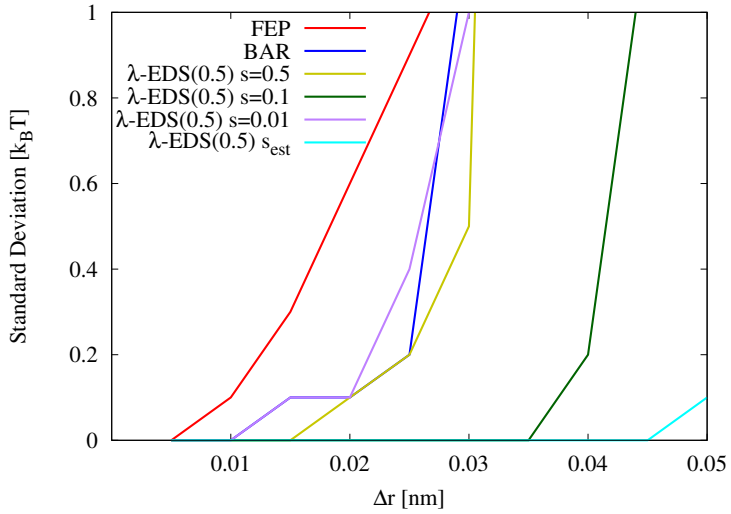

Figure 8: Standard deviations of free energy differences associated with changes Δr of the equilibrium bond length in a hypothetical molecule. The standard deviations are determined over ten repetitions of the calculations. The protocols involve: (*i*) FEP based on simulations of state A; (*ii*) BAR based on simulations of states A and B; (*iii*) λ-EDS(0.5) simulations with $s = 0.5$, 0.1, 0.01, and s_{est} using FEP.

shifts in the dihedral potential. The panels at the top show the potential energy surfaces of states A (left) and B (right). The four energy minima (blue) of one state correspond to the

four energy maxima (pink) of the other state (accounting for periodicity). The free energy difference is zero due to symmetry. The remaining panels are arranged in three columns, corresponding to different barrier heights $\Delta V_{barrier}$ of 5, 20, or 50 $k_{\mathrm{B}}T$. The five rows show the potential energy surfaces of λ-EDS(0.5) with s-values decreasing from 1 to 0.01, as well as the $\Delta V_{barrier}$-dependent s_{est} value from Eq. 16.

In contrast to the potential energy surfaces of the end states, the λ-EDS surfaces exhibit eight energy minima, because they trace the lowest potential energy among the two end states. The surfaces become progressively flatter as the s-value decreases. The potential energy surfaces with $s = 0.01$ and $\Delta V_{barrier} = 5$, and 20 $k_{\mathrm{B}}T$ are almost entirely flat, because λ-EDS becomes very similar to EI with $\lambda = 0.5$, and the corresponding linear combination of the potential energies is zero by symmetry. This is clearly inefficient for a free energy calculation, since a significant fraction of the sampling occurs in high energy regions. The use of the $\Delta V_{barrier}$-dependent value s_{est} from Eq. 16 leads to nearly identical surfaces in terms of the $\Delta V_{barrier}$-scaled potential energy. The residual free energy barriers on these λ-EDS surfaces are expected to represent a reasonable compromise between statistical efficiency and barrier crossing for a given $\Delta V_{barrier}$.

The average errors of the calculated free energy differences, along with their error bars, are reported in Table 4. Except for the last entry, all results are based on λ-EDS(0.5) calculations at the specified s-value with the FEP estimator. For the system with a low energy barrier of 5 $k_{\mathrm{B}}T$, all s-values lead to accurate and precise results. However, the lowest s-values of 0.025 and 0.01 exhibit slightly higher error bars. For the intermediate energy barrier of 20 $k_{\mathrm{B}}T$, which corresponds to barriers encountered in some amino acid side chains,[6,63,113,114] only s-values of 0.1 or below lead to acceptable results, as the simulations with higher s-values are less able to cross the energy barriers. For the highest barrier $\Delta V_{barrier}$ of 50 $k_{\mathrm{B}}T$, only $s = 0.01$ leads to accurate and precise results. While s_{est} gives adequate results for $\Delta V_{barrier}$ values of 5 and 20 $k_B T$, an increased error is observed for the barrier of 50 $k_B T$. This shows the limitations of the approach outlined in Fig. 5c.

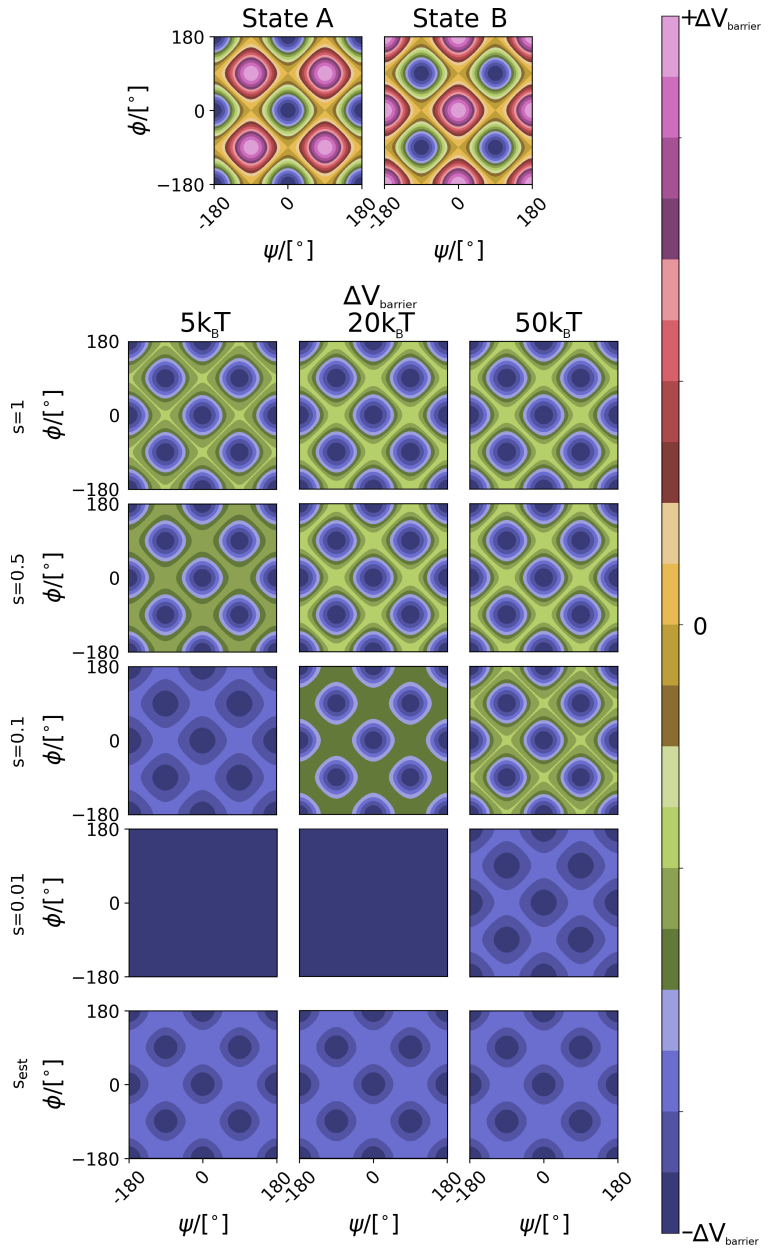

Figure 9: Potential energy surfaces of λ-EDS(0.5) for the mutation of a two-dimensional dihedral potential. The panels at the top show the potential energy surfaces of the initial state A (left) and of the final state B (right). The remaining panels are arranged in three columns, corresponding to different barrier heights $\Delta V_{barrier}$ of 5, 20, or 50 $k_\mathrm{B}T$, and five rows corresponding to λ-EDS(0.5) with $s = 1$, 0.5, 0.25, 0.1, 0.05, 0.025, 0.01, as well as the $\Delta V_{barrier}$-dependent s_est value from Eq. 16 ($s = 0.122$, 0.03 or 0.012 for the three increasing $\Delta V_{barrier}$ values). The color schemes are scaled according to the respective $\Delta V_{barrier}$.

The last entry in Table 4 corresponds to a RE-EDS simulation[75,76] with two replicas at s-values of 0.01 and 0.5. This setup doubles the computational cost, but the procedure

is easily parallelized. The use of replicas with different s-values allows the combination to benefit from both the low variance of MVP at $s = 0.5$ and the more frequent transitions at the lower s-value. The results with RE-EDS are accurate for all $\Delta V_{barrier}$ values, and more precise than any scheme relying on a single s-value.

Table 4: Average errors of the calculated free energy differences for the mutation of a two-dimensional dihedral potential, considering three values for the energy barrier $\Delta V_{barrier}$. Here, states A and B correspond to opposite phase shifts in the dihedral potential. The errors are calculated relative to the analytical reference result of zero. The protocols involve: λ-EDS(0.5) simulations with $s = 1$, 0.5, 0.1, 0.01, 0.001, and s_{est}; RE-EDS simulations using two replicas with s-values of 0.5 and 0.01. The s_{est} value is based on $\Delta V_{barrier}$ according to Eq. 16 ($s = 0.122$, 0.03 or 0.012 for the three increasing $\Delta V_{barrier}$ values). N_{sim} is the required number of simulations. The error bars correspond to the standard deviations over ten repetitions. Accurate results (errors below $0.5\,k_{\text{B}}T$) are highlighted in boldface, and precise results (standard deviations below $0.5\,k_{\text{B}}T$) are underlined. All values are in $k_{\text{B}}T$.

		$\Delta V_{barrier}$		
Scheme	N_{sim}	5	20	50
λ-EDS(0.5), $s = 1$ (BBE)	1	$\underline{\mathbf{0.0 \pm 0.1}}$	1.2 ± 3.0	56.1 ± 5.9
λ-EDS(0.5), $s = 0.5$ (MVP)	1	$\underline{\mathbf{0.0 \pm 0.1}}$	0.5 ± 1.1	57.3 ± 5.2
λ-EDS(0.5), $s = 0.25$	1	$\underline{\mathbf{0.0 \pm 0.1}}$	$\mathbf{0.0 \pm 1.0}$	58.8 ± 3.2
λ-EDS(0.5), $s = 0.1$	1	$\underline{\mathbf{0.0 \pm 0.1}}$	$\underline{\mathbf{0.0 \pm 0.5}}$	57.5 ± 3.0
λ-EDS(0.5), $s = 0.05$	1	$\underline{\mathbf{0.1 \pm 0.1}}$	$\underline{\mathbf{0.1 \pm 0.3}}$	53.4 ± 7.0
λ-EDS(0.5), $s = 0.025$	1	$\underline{\mathbf{0.0 \pm 0.2}}$	$\underline{\mathbf{0.0 \pm 0.2}}$	16.9 ± 22.0
λ-EDS(0.5), $s = 0.01$	1	$\underline{\mathbf{-0.1 \pm 0.2}}$	$\underline{\mathbf{0.0 \pm 0.3}}$	$\underline{\mathbf{-0.2 \pm 0.4}}$
λ-EDS(0.5), s_{est}	1	$\underline{\mathbf{0.0 \pm 0.1}}$	$\underline{\mathbf{0.0 \pm 0.3}}$	$\mathbf{0.4 \pm 1.1}$
RE-EDS, $s_1 = 0.5, s_2 = 0.01$	2	$\underline{\mathbf{0.1 \pm 0.1}}$	$\underline{\mathbf{0.0 \pm 0.1}}$	$\underline{\mathbf{-0.1 \pm 0.3}}$

Lennard-Jones Particles in Water

The last benchmark system mimics the cavity creation process in absolute free energy calculations, such as solvation free energies,[69,115–118] or ligand binding.[119–121] This is equivalent to finding the probability of the spontaneous formation of a ligand-sized cavity in the corresponding environment.[122] The chemical potential of the cavity is roughly proportional to its volume.[123,124] Therefore, free energy methods that can achieve larger effective volume changes per step will require fewer intermediate steps to reach the ligand size. This capabil-

ity is tested here with the creation of Lennard-Jones (LJ) particles in water, using effective radii between 0.05 and 0.40 nm (corresponding to effective volume changes between 0.0005 and 0.268 nm^3 per step).

The average errors of the calculated free energy change for the creation of a LJ particle in water are reported in Table 5. Here, state A corresponds to a dummy atom and state B to a LJ particle of effective radius S. The errors are calculated relative to accurate reference calculations.

The first entry in Table 5 corresponds to FEP estimates based on simulations of state B. The results are inaccurate and imprecise for all radii, because the repulsion precludes any significant phase space overlap with water molecules at the center of the particle. This results in a bias of the calculated free energy difference, and the errors are systematically becoming more negative with increasing S.

The second entry corresponds to SCP simulations with the FEP estimator. By using SCP and sufficiently small radii, water molecules are sometimes able to partially penetrate into the cavity, thus yielding accurate and precise results up to a radius of about 0.15 nm. Beyond this radius, the errors are again systematically too negative. Because the radius is smaller than that of a non-hydrogen atom, accurate free energy calculations require several intermediate states for the creation or annihilation of an atom when using a SCP scheme. In practice, SCP is often used for relative free energy calculations with different substituents,[125,126] where the solvent-accessible volume is partly occluded by neighboring non-vanishing atoms. Thus, in this situation, the SCP scheme is often sufficient to mutate one substituent into another in a single step. Enabling larger effective volume changes per λ-step would allow for the treatment of larger substituents, or even changes in the core regions.

The third entry corresponds to combining data from simulations at the end states with the BAR estimator. Although the computational cost is doubled, this approach represents a significant improvement over FEP and, to a lesser extent, SCP. The limiting cavity radius is now about 0.20 nm, which starts to be comparable to the radii of typical non-hydrogen

atoms. This observation is at the root of the serial insertion scheme[26] to avoid singularity issues in free energy calculations.

Finally, the four remaining entries are based on λ-EDS(0.5) simulations at different s-values. Using BBE ($s = 1.0$) or MVP (s=0.5) yields accurate and precise estimates for radii up to 0.15 nm. This is comparable to the SCP case, but the resulting errors are smaller. Using $s = 0.1$ leads to the best results, with a limiting radius of 0.25 nm. This scheme is both less expensive and more accurate than BAR. The results with $s = 0.01$ are again worse, because this scheme behaves like EI with $\lambda = 0.5$.

Table 5: Average errors of calculated free energy change for the formation of a LJ particle in water, considering eight values for the effective cavity radius S. The errors are relative to accurate reference calculations. Here, state A corresponds to a dummy atom and state B to a LJ particle of effective radius S. The protocols involve: FEP based on simulations of state B; SCP with $\lambda = 0.5$ and FEP; BAR based on simulations of states A and B; λ-EDS(0.5) simulations with FEP and $s = 1$, 0.5, 0.1, and 0.01. N_{sim} is the number of necessary simulations. Accurate results (errors below 1.24 kJ mol^{-1} or 0.5 $k_{\mathrm{B}}T$) are highlighted in boldface, and precise results (standard deviations below 1.24 kJ mol^{-1}) are underlined. BAR calculations that did not converge within 500 iterations are indicated by crosses. All values are in kJ mol^{-1}.

		S [nm]							
	N_{sim}	0.05	0.10	0.15	0.20	0.25	0.30	0.35	0.40
FEP	1	−1.6	−3.8	−7.8	−12.7	−20.3	−30.5	−41.8	−53.5
SC	1	**−0.1**	**−0.4**	**−1.1**	−4.9	−10.1	−16.7	−26.1	−38.1
BAR	2	**0.0**	**0.0**	**0.1**	**−0.2**	1.5	4.8	−3.2	×
λ-EDS(0.5), $s = 1.0$	1	**0.0**	**0.0**	**0.2**	**0.1**	6.2	89.9	439.9	1518.0
λ-EDS(0.5), $s = 0.5$	1	**0.1**	**−0.1**	**0.1**	**0.3**	6.3	86.8	266.9	1309.1
λ-EDS(0.5), $s = 0.1$	1	**0.1**	**−0.1**	**0.2**	**−0.5**	**0.0**	96.0	356.4	1239.7
λ-EDS(0.5), $s = 0.01$	1	−1.4	−3.0	−5.6	−11.1	−16.9	24.7	114.1	861.1

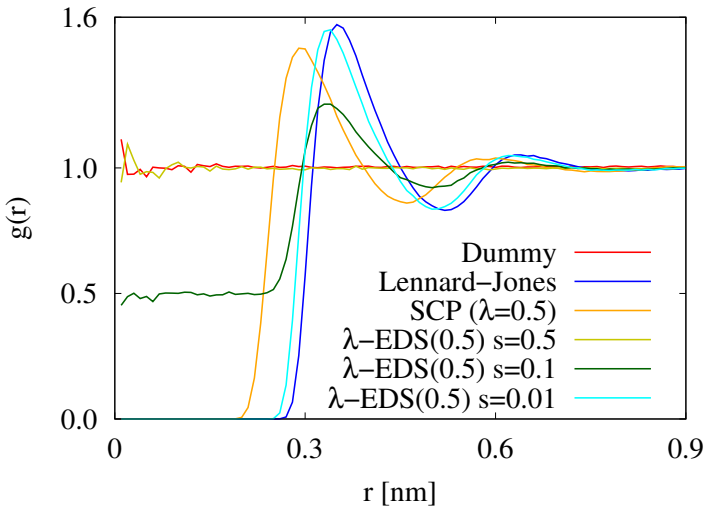

Figure 10: Radial distribution functions between the test particle and water oxygen atoms. The $g(r)$ functions are displayed as a function of distance r for a dummy particle, a LJ particle with an effective radius S of 0.2 nm, using a soft core potential, and using λ-EDS(0.5) with $s = 0.5$, 0.1, and 0.01.

The effect of the different s-values is also evidenced by the radial distribution functions $g(r)$ in Fig. 10 considering $S = 0.2\,\text{nm}$. The dummy state A (red curve) does not interact with water, resulting in an uniform $g(r)$ distribution. The physical LJ particle state B (blue curve) exhibits a peak centered at the minimum of the LJ potential at about 0.35 nm. Using SCP at $\lambda = 0.5$ shifts the peak of the radial distribution function to closer distances, but does not provide sufficient phase space overlap with the dummy state. For maximum efficiency, an intermediate state needs to encompass the relevant phase spaces of both states A and B to provide accurate free energy differences.[9,29,62] Analogously to Fig. 4a, λ-EDS(0.5) with $s = 0.5$ exhibits a very small energy barrier at short interparticle distances, which can be overcome by thermal motions. Thus, the $g(r)$ at $s = 0.5$ corresponds to the behavior of dummy atoms, which leads to a suboptimal performance because of insufficient sampling of the LJ particle state. The opposite is true for $s = 0.01$ (purple), which exhibits a $g(r)$ that corresponds more to a particle with EI at $\lambda = 0.5$. Since short interparticle distances are never sampled, the results with $s = 0.01$ are very similar to the poor results of FEP from state B. Employing λ-EDS with $s = 0.1$ (green) leads to a $g(r)$ that samples both

short interparticle distances and the energy minimum of the cavity potential. Therefore, the resulting free energy differences are both accurate and precise.

Conclusions

Based on previous ideas by Bennett,[29] Blondel,[51] Pham and Shirts,[45] Reinhardt and Grubmüller,[52] and Christ and van Gunsteren,[17,53] a new framework termed λ-EDS is introduced for the creation of intermediate states in alchemical free energy calculations. λ-EDS encompasses the EDS, MVP, and BBE methods as special cases. In the limit of $s \to 0$, it is equivalent to conventional TI with EI. It can also address the van der Waals endpoint problem like SCP. In addition, λ-EDS also offers the possibility to overcome sampling problems along the alchemical pathway.

It was found that the way intermediate states are created can have more influence on the convergence than the choice of the free energy estimator. For example, FEP calculations with one λ-EDS simulation oftentimes outperform the more efficient BAR estimator based on two conventional MD simulations. Like the softness parameter α in SCP, the smoothness parameter s in λ-EDS represents a key factor for the efficiency. λ-EDS either performs significantly better than conventional EI intermediate states, or yields exactly the same results in the limit $s \to 0$. The optimal choice of the s-value in terms of sampling depends on the height of the anticipated energy barriers. On the one hand, λ-EDS with high s-values (ca. 0.1 to 1) approaches the efficiency of the MVP and produces SCP in the context of dummy atoms. However, high energy barriers might still be present in such simulations. On the other hand, λ-EDS with low s-values (ca. 0.01 or lower) approaches the behavior of conventional EI intermediate states, which is less favorable in terms of variance and inadequate in the case of dummy atom creation, but leads to lower energy barriers. Thus, alchemical transformations with high energy barriers, such as those altering the covalent or electrostatic interactions, are best performed with a low s-value, whereas cavity creation

converges better with a relatively high s-value. Using an s-value of ca. 0.1 might be a reasonable compromise in some cases as it provides the best overall results for the considered benchmark systems. One can also use a free energy protocol that splits the alchemical pathway into at least two parts. First, scaling the charges using EI (with low s-values), and, second, transforming the van der Waals interactions using SCP (with high s-values). Notably, such a splitting is already common practice in the field.[127,128] Instead of simulating two separate steps, one could also envision using different s-values for each interaction type in one free energy simulation, or varying the s-value along the alchemical pathway.

One particularly attractive feature of λ-EDS is its ability to emulate SCP while remaining separable in λ. This avoids the need of dedicated free energy code in the nonbonded routines and minimizes the computational overhead in the calculation of these interactions. This is particularly advantageous for efficient free energy estimators such as BAR and MBAR, as the λ-EDS Hamiltonian can be recalculated at any λ-point without further energy evaluations. Finally, the implementation of λ-EDS in a simulation program is rather straightforward, as it only affects the combination of the end state potential energies, forces, and virials. This simplicity is also evidenced by the fact that three different programs (GROMOS, CHARMM, and Ensembler) were employed in this manuscript. Owing to these properties, λ-EDS promises to become a very useful scheme in the field of free energy calculations.

Acknowledgement

The authors would like to thank Clara Christ, Michael Shirts, Martin Reinhardt and Helmut Grubmüller for valuable discussions. S.R. gratefully acknowledges financial support by the Swiss National Science Foundation (Grant Number 200021-178762) and by ETH Zurich (ETH-34 17-2). P.H. is thankful for financial support by the Swiss National Science Foundation (Grant Number 200021-175944).

References

(1) Christ, C. D.; Mark, A. E.; van Gunsteren, W. F. Basic ingredients of free energy calculations: A review. *J. Comput. Chem.* **2010**, *31*, 1569–1582.

(2) Hansen, N.; van Gunsteren, W. F. Practical aspects of free-energy calculations: A review. *J. Chem. Theory Comput.* **2014**, *10*, 2632–2647.

(3) Armacost, K. A.; Riniker, S.; Cournia, Z. Novel directions in free energy methods and applications. *J. Chem. Inf. Model.* **2020**, *60*, 1–5.

(4) Bieler, N. S.; Hünenberger, P. H. Orthogonal sampling in free-energy calculations of residue mutations in a tripeptide: TI vs. λ-LEUS. *J. Comput. Chem.* **2015**, *36*, 1686–1697.

(5) Graf, M. M. H.; Maurer, M.; Oostenbrink, C. Free-energy calculations of residue mutations in a tripeptide using various methods to overcome inefficient sampling. *J. Comput. Chem.* **2016**, *37*, 2597–2605.

(6) Hahn, D. F.; König, G.; Hünenberger, P. H. Overcoming orthogonal barriers in alchemical free-energy calculations: On the relative merits of λ-variations, λ-extrapolations, and biasing. *J. Chem. Theory Comput.* **2020**, *16*, 1630–1645.

(7) Wu, D.; Kofke, D. A. Phase-space overlap measures. I. Fail-safe bias detection in free energies calculated by molecular simulation. *J. Chem. Phys.* **2005**, *123*, 054103.

(8) Wu, D.; Kofke, D. A. Phase-space overlap measures. II. Design and implementation of staging methods for free-energy calculations. *J. Chem. Phys.* **2005**, *123*, 084109.

(9) König, G.; Brooks, B. R.; Thiel, W.; York, D. M. On the convergence of multi-scale free energy simulations. *Mol. Simul.* **2018**, *44*, 1062–1081.

(10) Jorgensen, W. L.; Ravimohan, C. Monte Carlo simulation of differences in free energies of hydration. *J. Phys. Chem.* **1985**, *83*, 3050–3054.

(11) Straatsma, T. P.; McCammon, J. A. Multiconfiguration thermodynamic integration. *J. Chem. Phys.* **1991**, *95*, 1175–1188.

(12) Valleau, J. P.; Card, D. N. Monte Carlo estimation of the free energy by multistage sampling. *J. Chem. Phys.* **1972**, *57*, 5457–5462.

(13) Lu, N.; Kofke, D. A.; Woolf, T. B. Staging is more important than perturbation method for computation of enthalpy and entropy changes in complex systems. *J. Phys. Chem. B* **2003**, *107*, 5598–5611.

(14) Pohorille, A.; Jarzynski, C.; Chipot, C. Good practices in free-energy calculations. *J. Phys. Chem. B* **2010**, *114*, 10235–10253.

(15) Oostenbrink, C.; van Gunsteren, W. F. Single-step perturbations to calculate free energy differences from unphysical reference states: limits on size, flexibility and character. *J. Comput. Chem.* **2003**, *24*, 1730–1739.

(16) Oostenbrink, C. In *Computational drug discovery and design.*; Baron, R., Ed.; Humana press (Springer), New York, USA, 2012.

(17) Christ, C. D.; van Gunsteren, W. F. Enveloping distribution sampling: A method to calculate free energy differences from a single simulation. *J. Chem. Phys.* **2007**, *126*, 184110.

(18) Hansen, N.; Hünenberger, P. H.; van Gunsteren, W. F. Efficient combination of environment change and alchemical perturbation within the enveloping distribution sampling (EDS) scheme: Twin-system EDS and application to the determination of octanol-water partition coefficients. *J. Chem. Theory Comput.* **2013**, *9*, 1334–1346.

(19) Bieler, N. S.; Tschopp, J. P.; Hünenberger, P. H. Multistate λ-local-elevation umbrella-sampling (MS-λ-LEUS): Method and application to the complexation of cations by crown ethers. *J. Chem. Theory Comput.* **2015**, *11*, 2575–2588.

(20) Hahn, D. F.; Hünenberger, P. H. Alchemical free-energy calculations by multiple-replica λ-dynamics: The conveyor belt thermodynamic integration (CBTI) scheme. *J. Chem. Theory Comput.* **2019**, *15*, 2392–2419.

(21) Hahn, D. F.; Zarotiadis, R. A.; Hünenberger, P. H. The conveyor belt umbrella sampling (CBUS) scheme: Principle and application to the calculation of the absolute binding binding free energies of alkali cations to crown ethers. *J. Chem. Theory Comput.* **2020**, *16*, 2474–2493.

(22) Kirkwood, J. G. Statistical mechanics of fluid mixtures. *J. Chem. Phys.* **1935**, *3*, 300–313.

(23) Jorgensen, W. L.; Thomas, L. L. Perspective on free-energy perturbation calculations for chemical equilibria. *J. Chem. Theory Comput.* **2008**, *4*, 869–876.

(24) Cross, A. J. Influence of Hamiltonian parameterization on convergence of Kirkwood free energy calculations. *Chem. Phys. Lett.* **1986**, *128*, 198–202.

(25) Mezei, M.; Beveridge, D. L. In *Computer simulation of chemical and biomolecular systems, in Annals of the New York Academy of Sciences*; Beveridge, D. L., Jorgensen, W. L., Eds.; The New York Academy of Sciences, New York, USA, 1986; Vol. 482.

(26) Boresch, S.; Bruckner, S. Avoiding the van der Waals endpoint problem using serial atomic insertion. *J. Comput. Chem.* **2011**, *32*, 2449–2458.

(27) Giese, T. J.; York, D. M. A GPU-accelerated parameter interpolation thermodynamic integration free energy method. *J. Chem. Theory Comput.* **2018**, *14*, 1564–1582.

(28) Zwanzig, R. W. High-temperature equation of state by a perturbation method. I. Nonpolar gases. *J. Chem. Phys.* **1954**, *22*, 1420–1426.

(29) Bennett, C. H. Efficient estimation of free energy differences from Monte Carlo data. *J. Comput. Phys.* **1976**, *22*, 245–268.

(30) Shirts, M. R.; Bair, E.; Hooker, G.; Pande, V. S. Equilibrium free energies from nonequilibrium measurements using maximum-likelihood methods. *Phys. Rev. Lett.* **2003**, *91*, 140601.

(31) Shirts, M. R.; Chodera, J. D. Statistically optimal analysis of samples from multiple equilibrium states. *J. Chem. Phys.* **2008**, *129*, 124105.

(32) Torrie, G. M.; Valleau, J. P. Nonphysical sampling distributions in Monte Carlo free-energy estimation: Umbrella sampling. *J. Comput. Phys.* **1977**, *23*, 187–199.

(33) Mruzik, M. R.; Abraham, F. F.; Schreiber, D. E.; Pound, G. M. A Monte Carlo study of ion-water clusters. *J. Chem. Phys.* **2006**, *64*, 481–491.

(34) Simonson, T. Free energy of particle insertion. An exact analysis of the origin singularity for simple liquids. *Mol. Phys.* **1993**, *80*, 441–447.

(35) Beutler, T. C.; Mark, A. E.; van Schaik, R.; Gerber, P. R.; van Gunsteren, W. F. Avoiding singularities and numerical instabilities in free energy calculations based on molecular simulations. *Chem. Phys. Lett.* **1994**, *222*, 529–539.

(36) Zacharias, M.; Straatsma, T. P.; McCammon, J. A. Separation-shifted scaling, a new scaling method for Lennard-Jones interactions in thermodynamic integration. *J. Chem. Phys.* **1994**, *100*, 9025–9031.

(37) Pearlman, D. A.; Kollman, P. A. A new method for carrying out free energy perturbation calculations: Dynamically modified windows. *J. Chem. Phys.* **1989**, *90*, 2460–2470.

(38) Straatsma, T. P.; Zacharias, M.; McCammon, J. A. Holonomic constraint contributions to free energy differences from thermodynamic integration molecular dynamics simulations. *Chem. Phys. Lett.* **1992**, *196*, 297–302.

(39) Sun, X.; Spellmeyer, D.; Pearlman, D. A.; Kollman, P. Simulation of the solvation free energies for methane, ethane, and propane and corresponding amino acid dipeptides: A critical test of the "bond-PMF" correction, a new set of hydrocarbon parameters, and the gas phase-water hydrophobicity scale. *J. Am. Chem. Soc.* **1992**, *114*, 6798–6801.

(40) Lee, J.; Tofoleanu, F.; IV, F. C. P.; König, G.; Huang, J.; Damjanović, A.; Baek, M.; Seok, C.; Brooks, B. R. Absolute binding free energy calculations of CBClip host-guest systems in the SAMPL5 blind challenge. *J. Comput. Aided Mol. Des.* **2017**, *31*, 71–85.

(41) Tofoleanu, F.; Lee, J.; IV, F. C. P.; König, G.; Huang, J.; Baek, M.; Seok, C.; Brooks, B. R. Absolute binding free energies for octa-acids and guests in SAMPL5. *J. Comput. Aided Mol. Des.* **2017**, *31*, 107–118.

(42) Naden, L. N.; Pham, T. T.; Shirts, M. R. Linear basis function approach to efficient alchemical free energy calculations. 1. Removal of uncharged atomic sites. *J. Chem. Theory Comput.* **2014**, *10*, 1128–1149.

(43) Naden, L. N.; Shirts, M. R. Linear basis function approach to efficient alchemical free energy calculations. 2. Inserting and deleting particles with Coulombic interactions. *J. Chem. Theory Comput.* **2015**, *11*, 2536–2549.

(44) Pham, T. T.; Shirts, M. R. Identifying low variance pathways for free energy calculations of molecular transformations in solution phase. *J. Chem. Phys.* **2011**, *135*, 034114.

(45) Pham, T. T.; Shirts, M. R. Optimal pairwise and non-pairwise alchemical pathways

for free energy calculations of molecular transformations in solution phase. *J. Chem. Phys.* **2012**, *136*, 124120.

(46) Gapsys, V.; Seeliger, D.; de Groot, B. L. New soft-core potential function for molecular dynamics based alchemical free energy calculations. *J. Chem. Theory Comput.* **2012**, *8*, 2373–2382.

(47) Buelens, F. P.; Grubmüller, H. Linear-scaling soft-core scheme for alchemical free energy calculations. *J. Comput. Chem.* **2012**, *33*, 25–33.

(48) Pal, R. K.; Gallicchio, E. Perturbation potentials to overcome order/disorder transitions in alchemical binding free energy calculations. *J. Chem. Phys.* **2019**, *151*, 124116.

(49) Lee, T.-S.; Lin, Z.; Allen, B. K.; Lin, C.; Radak, B. K.; Tao, Y.; Tsai, H.-C.; Sherman, W.; York, D. M. Improved Alchemical Free Energy Calculations with Optimized Smoothstep Softcore Potentials. *J. Chem. Theory Comput.* **2020**,

(50) Gallicchio, E. Alchemical Transformations for Single-Step Hydration Free Energy Calculations. *arXiv preprint arXiv:2005.06504* **2020**,

(51) Blondel, A. Ensemble variance in free energy calculations by thermodynamic integration: theory, optimal "alchemical" path, and practical solutions. *J. Comput. Chem.* **2004**, *25*, 985–993.

(52) Reinhardt, M.; Grubmüller, H. Determining Free Energy Differences Through Variationally-Derived Intermediates. *J. Chem. Theory Comput.* **2020**, *16*, 3504–3512.

(53) Christ, C. D.; van Gunsteren, W. F. Multiple free energies from a single simulation: Extending enveloping distribution sampling to nonoverlapping phase-space distributions. *J. Chem. Phys.* **2008**, *128*, 174112.

(54) Christ, C. D.; van Gunsteren, W. F. Comparison of three enveloping distribution

sampling Hamiltonians for the estimation of multiple free energy differences from a single simulation. *J. Comput. Chem.* **2009**, *30*, 1664–1679.

(55) Hummer, G.; Szabo, A. Calculation of free-energy differences from computer simulations of initial and final states. *J. Chem. Phys.* **1996**, *105*, 2004–2010.

(56) Jorge, M.; Garrido, N. M.; Queimada, A. J.; Economou, I. G.; Macedo, E. A. Effect of the integration method on the accuracy and computational efficiency of free energy calculations using thermodynamic integration. *J. Chem. Theory Comput.* **2010**, *6*, 1018–1027.

(57) Bruckner, S.; Boresch, S. Efficiency of alchemical free energy simulations. I. A practical comparison of the exponential formula, thermodynamic integration, and Bennett's acceptance ratio method. *J. Comput. Chem.* **2011**, *32*, 1303–1319.

(58) Bruckner, S.; Boresch, S. Efficiency of alchemical free energy simulations. II. Improvements for thermodynamic integration. *J. Comput. Chem.* **2011**, *32*, 1320–1333.

(59) Shyu, C.; Ytreberg, F. M. Reducing the bias and uncertainty of free energy estimates by using regression to fit thermodynamic integration data. *J. Comput. Chem.* **2009**, *30*, 2297–2304.

(60) Vilseck, J. Z.; Acevedo, O. Computing free-energy profiles using multidimensional potentials of mean force and polynomial quadrature methods. *Annu. Rep. Comput. Chem.* **2010**, *6*, 37–49.

(61) Shyu, C.; Ytreberg, F. M. Accurate estimation of solvation free energy using polynomial fitting techniques. *J. Comput. Chem.* **2011**, *32*, 134–141.

(62) König, G.; Bruckner, S.; Boresch, S. Unorthodox uses of Bennett's acceptance ratio method. *J. Comput. Chem.* **2009**, *30*, 1712–1718.

(63) König, G.; Boresch, S. Non-Boltzmann sampling and Bennett's acceptance ratio method: How to profit from bending the rules. *J. Comput. Chem.* **2011**, *32*, 1082–1090.

(64) Steinbrecher, T.; Mobley, D. L.; Case, D. A. Nonlinear scaling schemes for Lennard-Jones interactions in free energy calculations. *J. Chem. Phys.* **2007**, *127*, 214108.

(65) Li, H.; Yang, W. Forging the missing link in free energy estimations: λ-WHAM in thermodynamic integration, overlap histogramming, and free energy perturbation. *Chem. Phys. Lett.* **2007**, *440*, 155–159.

(66) de Ruiter, A.; Oostenbrink, C. Extended thermodynamic integration: Efficient prediction of lambda derivatives at nonsimulated points. *J. Chem. Theory Comput.* **2016**, *12*, 4476–4486.

(67) Mark, A. E.; Xu, Y.; Liu, H.; van Gunsteren, W. F. Rapid non-empirical approaches for estimating relative binding free energies. *Acta Biochim. Pol.* **1995**, *42*, 525–536.

(68) Mark, A. E.; Schäfer, H.; Liu, H.; van Gunsteren, W. F. In *Computational molecular dynamics: challenges, methods, ideas, Proceedings of the 2nd Intl. Symp. on Algorithms for Macromol. Mod.*; Deuflhard, P., Hermans, J., Leimkuhler, B., Mark, A. E., Reich, S., Skeel, R. D., Eds.; Springer-Verlag, Berlin, Germany, 1999.

(69) Schäfer, H.; van Gunsteren, W. F.; Mark, A. E. Estimating relative free energies from a single ensemble: Hydration free energies. *J. Comput. Chem.* **1999**, *20*, 1604–1617.

(70) Mordasini, T. Z.; McCammon, J. A. Calculations of relative hydration free energies: A comparative study using thermodynamic integration and an extrapolation method based on a single reference state. *J. Phys. Chem. B 2000* **2000**, *104*, 360–367.

(71) Mori, T.; Hamers, R. J.; Pedersen, J. A.; Cui, Q. Integrated Hamiltonian sampling: A

simple and versatile method for free energy simulations and conformational sampling. *J. Phys. Chem. B* **2014**, *118*, 8210–8220.

(72) Lu, N.; Kofke, D. A. Accuracy of free-energy perturbation calculations in molecular simulation. I. Modeling. *J. Chem. Phys.* **2001**, *114*, 7303–7311.

(73) Lu, N.; Kofke, D. A. Accuracy of free-energy perturbation calculations in molecular simulation. II. Heuristics. *J. Chem. Phys.* **2001**, *115*, 6866–6875.

(74) Riniker, S.; Christ, C. D.; Hansen, N.; Mark, A. E.; Nair, P. C.; van Gunsteren, W. F. Comparison of enveloping distribution sampling and thermodynamic integration to calculate binding free energies of phenylethanolamine N-methyltransferase inhibitors. *J. Chem. Phys.* **2011**, *135*, 024105.

(75) Sidler, D.; Schwaninger, A.; Riniker, S. Replica exchange enveloping distribution sampling (RE-EDS): A robust method to estimate multiple free-energy differences from a single simulation. *J. Chem. Phys.* **2016**, *145*, 154114.

(76) Sidler, D.; Cristòfol-Clough, M.; Riniker, S. Efficient round-trip time optimization for replica-exchange enveloping distribution sampling (RE-EDS). *J. Chem. Theory Comput.* **2017**, *13*, 3020–3030.

(77) Perthold, J. W.; Oostenbrink, C. Accelerated enveloping distribution sampling: Enabling sampling of multiple end states while preserving local energy minima. *J. Phys. Chem. B* **2018**, *122*, 5030–5037.

(78) Åqvist, J.; Medina, C.; Samuelsson, J. E. A new method for predicting binding affinity in computer-aided drug design. *Protein Eng.* **1994**, *7*, 385–391.

(79) Hummer, G.; Pratt, L. R.; Garcia, A. E. Free energy of ionic hydration. *J. Phys. Chem.* **1996**, *100*, 1206–1215.

(80) Schmid, N.; Christ, C. D.; Christen, M.; Eichenberger, A. P.; van Gunsteren, W. F. Architecture, implementation and parallelisation of the GROMOS software for biomolecular simulation. *Comput. Phys. Commun.* **2012**, *183*, 890–903.

(81) Kunz, A. P. E.; Allison, J. R.; Geerke, D. P.; Horta, B. A. C.; Hünenberger, P. H.; Riniker, S.; Schmid, N.; van Gunsteren, W. F. New functionalities in the GROMOS biomolecular simulation software. *J. Comput. Chem.* **2012**, *33*, 340–353.

(82) Riniker, S.; Christ, C. D.; Hansen, H. S.; Hünenberger, P. H.; Oostenbrink, C.; Steiner, D.; van Gunsteren, W. F. Calculation of relative free energies for ligand-protein binding, solvation and conformational transitions using the GROMOS biomolecular simulation software. *J. Phys. Chem. B* **2011**, *115*, 13570–13577.

(83) Berendsen, H. J. C.; Postma, J. P. M.; van Gunsteren, W. F.; di Nola, A.; Haak, J. R. Molecular dynamics with coupling to an external bath. *J. Chem. Phys.* **1984**, *81*, 3684–3690.

(84) Kepler, J. *Nova Stereometria Doliorum Vinariorum*; Johannes Plancus, Linz, 1615.

(85) Brooks, B. R.; Bruccoleri, R. E.; Olafson, B. D.; States, D. J.; Swaminathan, S.; Karplus, M. CHARMM: A program for macromolecular energy, minimization and dynamics calculations. *J. Comput. Chem.* **1983**, *4*, 187–217.

(86) Brokaw, J. B.; Haas, K. R.; Chu, J. W. Reaction path optimization with holonomic constraints and kinetic energy potentials. *J. Chem. Theory Comput.* **2009**, *5*, 2050–2061.

(87) König, G.; Miller, B. T.; Boresch, S.; Wu, X.; Brooks, B. R. Enhanced sampling in free energy calculations: Combining SGLD with the Bennett's acceptance ratio and enveloping distribution sampling methods. *J. Chem. Theory Comput.* **2012**, *8*, 3650–3662.

(88) Lee, J.; Miller, B. T.; Damjanović, A.; Brooks, B. R. Constant pH molecular dynamics in explicit solvent with enveloping distribution sampling and Hamiltonian exchange. *J. Chem. Theory Comput.* **2014**, *10*, 2738–2750.

(89) Lee, J.; Miller, B. T.; Damjanović, A.; Brooks, B. R. Enhancing constant-pH simulation in explicit solvent with a two-dimensional replica exchange method. *J. Chem. Theory Comput.* **2015**, *11*, 2560–2574.

(90) Lee, J.; Miller, T.; Brooks, B. R. Computational scheme for pH-dependent binding free energy calculation with explicit solvent. *Protein Sci.* **2016**, *25*, 231–243.

(91) Woodcock, H. L.; Miller, B. T.; Hodoscek, M.; Okur, A.; Larkin, J. D.; Ponder, J. W.; Brooks, B. R. MSCALE: A general utility for multiscale modeling. *J. Chem. Theory Comput.* **2011**, *7*, 1208–1219.

(92) König, G.; Pickard, F. C.; Huang, J.; Thiel, W.; MacKerell, A. D.; Brooks, B. R.; York, D. M. A Comparison of QM/MM simulations with and without the Drude oscillator model based on hydration free energies of simple solutes. *Molecules* **2018**, *23*, 2695.

(93) Herschbach, D. R.; Johnston, H. S.; Rapp, D. Molecular partition functions in terms of local properties. *J. Chem. Phys.* **1959**, *31*, 1652–1661.

(94) Boresch, S.; Karplus, M. The Jacobian factor in free energy simulations. *J. Chem. Phys.* **1996**, *105*, 5145–5154.

(95) Boresch, S.; Karplus, M. The role of bonded terms in free energy simulations: 1. Theoretical analysis. *J. Phys. Chem. A* **1999**, *103*, 103–118.

(96) Boresch, S.; Karplus, M. The role of bonded terms in free energy simulations. 2. Calculation of their influence on free energy differences of solvation. *J. Phys. Chem. A* **1999**, *103*, 119–136.

(97) König, G.; Brooks, B. R. Correcting for the free energy costs of bond or angle constraints in molecular dynamics simulations. *Biochim. Biophys. Acta* **2015**, *1850*, 932–943.

(98) Schroeder, B.; Hahn, D. Ensembler. `https://github.com/rinikerlab/Ensembler`, 2020.

(99) Metropolis, N.; Rosenbluth, A. W.; Rosenbluth, M. N.; Teller, A. H.; Teller, E. Equation of state calculations by fast computing machines. *J. Chem. Phys.* **1953**, *21*, 1087–1092.

(100) Sugita, Y.; Okamoto, Y. Replica-exchange molecular dynamics method for protein folding. *Chem. Phys. lett.* **1999**, *134*, 141–151.

(101) Fukunishi, H.; Watanabe, O.; Takada, S. On the Hamiltonian replica exchange method for efficient sampling of biomolecular systems: Application to protein structure prediction. *J. Chem. Phys.* **2002**, *116*, 9058–9067.

(102) Zhang, B. W.; Dai, W.; Gallicchio, E.; He, P.; Xia, J.; Tan, Z.; Levy, R. M. Simulating replica exchange: Markov state models, proposal schemes, and the infinite swapping limit. *J. Phys. Chem. B* **2016**, *120*, 8289–8301.

(103) Jorgensen, W. L.; Chandrasekhar, J.; Madura, J. D.; Impey, R. W.; Klein, M. L. Comparison of simple potential functions for simulating liquid water. *J. Chem. Phys.* **1983**, *79*, 926–935.

(104) Nosé, S. A molecular dynamics method for simulations in the canonical ensemble. *Mol. Phys.* **1984**, *52*, 255–268.

(105) Hoover, W. G. Canonical dynamics: Equilibrium phase-space distributions. *Phys. Rev. A* **1985**, *31*, 1695–1697.

(106) Ryckaert, J. P.; Ciccotti, G.; Berendsen, H. J. C. Numerical integration of the Cartesian equations of motion of a system with constraints: Molecular dynamics of n-alkanes. *J. Comput. Phys.* **1977**, *23*, 327–341.

(107) Steinbach, P. J.; Brooks, B. R. New spherical-cutoff methods for long-range forces in macromolecular simulation. *J. Comput. Chem.* **1994**, *15*, 667–683.

(108) Lu, N.; Singh, J. K.; Kofke, D. A. Appropriate methods to combine forward and reverse free-energy perturbation averages. *J. Chem. Phys.* **2003**, *118*, 2977–2984.

(109) Shirts, M. R.; Pande, V. S. Comparison of efficiency and bias of free energies computed by exponential averaging, the Bennett acceptance ratio, and thermodynamic integration. *J. Chem. Phys.* **2005**, *122*, 144107.

(110) König, G.; Brooks, B. R. Predicting binding affinities of host-guest systems in the SAMPL3 blind challenge: The performance of relative free energy calculations. *J. Comput. Aided Mol. Des.* **2012**, *26*, 543–550.

(111) de Ruiter, A.; Boresch, S.; Oostenbrink, C. Comparison of thermodynamic integration and Bennett's acceptance ratio for calculating relative protein-ligand binding free energies. *J. Comput. Chem.* **2013**, *34*, 1024–1034.

(112) Vanommeslaeghe, E. H.; Acharya, C.; Kundu, S.; Zhong, S.; Jhim, E.; Darian, E.; Guvench, O.; Lopes, P.; Vorobyov, I.; Jr., A. D. M. CHARMM General Force Field: A force field for drug-like molecules compatible with the CHARMM all-atom additive biological force fields. *J. Comput. Chem.* **2009**, *31*, 671–690.

(113) Leitgeb, M.; Schröder, C.; Boresch, S. Alchemical free energy calculations and multiple conformational substates. *J. Chem. Phys.* **2005**, *122*, 084109.

(114) König, G.; Bruckner, S.; Boresch, S. Absolute hydration free energies of blocked amino acids: Implications for protein solvation and stability. *Biophys. J.* **2013**, *104*, 453–462.

(115) Shirts, M. R.; Pitera, J. W.; Swope, W. C.; Pande, V. S. Extremely precise free energy calculations of amino acid side chain analogs: Comparison of common molecular mechanics force fields for proteins. *J. Chem. Phys.* **2003**, *119*, 5740–5761.

(116) Shivakumar, S.; Deng, Y.; Roux, B. Computations of absolute solvation free energies of small molecules using explicit and implicit solvent model. *J. Chem. Theory Comput.* **2009**, *5*, 919–930.

(117) König, G.; Reetz, M. T.; Thiel, W. 1-butanol as a solvent for efficient extraction of polar compounds from aqueous medium: Theoretical and practical aspects. *J. Phys. Chem. B* **2018**, *122*, 6975–6988.

(118) Pitera, J. W.; van Gunsteren, W. F. One-step perturbation methods for solvation free energies of polar solutes. *J. Phys. Chem.* **2001**, *105*, 11264–11274.

(119) Boresch, S.; Tettinger, F.; Leitgeb, M.; Karplus, M. Absolute binding free energies: A quantitative approach for their calculation. *J. Phys. Chem. B* **2003**, *107*, 9535–9551.

(120) Woo, H. J.; Roux, B. Calculation of absolute protein-ligand binding free energy from computer simulations. *Proc. Natl. Acad. Sci. USA* **2005**, *102*, 6825–6830.

(121) Gumbart, J. C.; Roux, B.; Chipot, C. Standard binding free energies from computer simulations: What is the best strategy? *J. Chem. Theory Comput.* **2013**, *9*, 794–802.

(122) Hummer, G.; Garde, S.; Garcia, A. E.; Pohorille, A.; Pratt, L. R. An information theory model of hydrophobic interactions. *Proc. Natl. Acad. Sci. USA 93* **1996**, *8951-8955*.

(123) Hummer, G.; Garde, S.; Garcıa, A.; Pratt, L. New perspectives on hydrophobic effects. *Chem. Phys.* **2000**, *258*, 349–370.

(124) Pitera, J. W.; van Gunsteren, W. F. The importance of solute-solvent van der Waals

interactions with interior atoms of biopolymers. *J. Am. Chem. Soc.* **2001**, *123*, 3163–3164.

(125) Oostenbrink, C.; van Gunsteren, W. F. Free energies of binding of polychlorinated biphenyls to the estrogen receptor from a single simulation. *Proteins: Struct. Func. Genet.* **2004**, *54*, 237–246.

(126) Nørholm, A. B.; Francotte, P.; Goffin, E.; Botez, I.; Danober, L.; Lestage, P.; Pirotte, B.; Kastrup, J. S.; Olsen, L.; Oostenbrink, C. Thermodynamic characterization of new positive allosteric modulators binding to the glutamate receptor A2 ligand-binding domain: Combining experimental and computational methods unravels differences in driving forces. *J. Chem. Inf. Model.* **2014**, *54*, 3404–3416.

(127) Deng, Y.; Roux, B. Hydration of amino acid side chains: Nonpolar and electrostatic contributions calculated from staged molecular dynamics free energy simulations with explicit water molecules. *J. Phys. Chem. B* **2004**, *108*, 16567–16576.

(128) Klimovich, P. V.; Shirts, M. R.; Mobley, D. L. Guidelines for the analysis of free energy calculations. *J. Comput. Aided Mol. Des.* **2015**, *29*, 397–411.

For Table of Contents Only

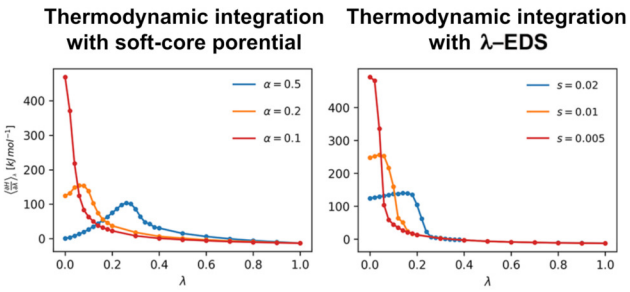

$$H_{\lambda-\mathrm{EDS}}(\lambda) = -\left[\beta s(\lambda)\right]^{-1} \ln\left\{(1-\lambda)\, e^{-\beta s(\lambda) H_A} + \lambda\, e^{-\beta s(\lambda)\left[H_B - E(\lambda)\right]}\right\}$$